THE UNIVERSITY OF QUEENSLAND

Development of Binder in Li-S Battery

Student Name: Mingwei, HU

Course Code: MECH 4501

Supervisor: Dr. Ruth Knibbe

Submission date: 30th May 2019

Faculty of Engineering, Architecture and Information Technology

Acknowledgement

This work would not have been possible without supervision from my supervisor, Dr. Ruth Knibbe, to who I would express my most sincere gratitude. I especially appreciated for her proposal of this project topic, guidance on entire experiments and comprehensive knowledge and suggestions about issues I encountered throughout the project.

I am grateful to all co-workers in the laboratory for assistance on the operation of apparatuses. I would also show my gratitude to Ahad, Lingbin, Zhila, Rana, and Ming for their insightful suggestions, explanation of battery theories and preparation of materials during my experiments.

Finally, I would like to thank my parents, wife, and friends for their endless supports and instructions during my entire thesis project.

Abstract

Since state-of-art Lithium-Ion battery (LIB) cannot satisfy people's demand gradually, more investigations emphasis on the development of Lithium Sulfur battery (LSB). As the competitive candidate, LSB possesses higher specific capacity (reaches 1672 mAh/g), cost-efficient material and safer operating voltage [1-3]. However, LSB still has several drawbacks preventing it from commercialization. The first major challenge is the low electrical conductivity of the sulfur element [3] and the second one is the polysulfide shuttle effect. Ling's team [2] found that by substituting traditional binder with carrageenan in the cathode, aforesaid problems can be alleviated, resulting in a better electrochemical performance of LSB. Carrageenan is a generic term of polysaccharide obtained from red seaweeds [4]. Its property of water solubility and strong adhesive strength stabilizes its functionality as a binder [2]. This project will focus on the development of iota and kappa carrageenan (iCar and kCar) binder in LSB with comparison to conventional PVDF binder.

The viscosity of carrageenan solutions was initially investigated. The gel structure did not retrograde over 7 days' observation, which proves that the viscosity of carrageenan solutions was less time-dependent. Meanwhile, the high fluidity of old kCar solution and gel structure within new kCar solution were both invalid to fabricate into qualified cathodes, causing batteries with only iCar and PVDF binders.

Cathode with 1.75 wt% iCar exhibited good adhesion between the cathode layer and current collector. SEM analysis also discovered more cracks and defects generated on PVDF based cathodes due to its inferior adhesive strength. Meanwhile, EDS results displayed excessive sulfur elements in cathode without being adjacent to the conductive network.

By evaluating the drying temperature of vacuum oven, well-conditioned iCar based batteries were fabricated without the presence of moisture and tested in comparison with PVDF based cells. Although iCar based cells did not deliver most energy densities, which were 511 mAh/g and 457 mAh/g for 5 wt% and 10 wt% binder composition, they presented better capacity retention rate of 63% and 77% after 150 cycles. Higher iCar binder content also resulted in higher capacity retention. This phenomenon indicated that iCar binder could sufficiently alleviate the polysulfide shuttling effect in LSB, which was also proven by higher R_{CT} in EIS testing.

Table of Contents

List of Figures

List of Tables

1 Introduction

1.1Background

Along with the intensive demand for high-performance battery utilized for portable electronics, home power storage and electric vehicles (EVs), lithium battery industry experienced rapid development during past decades. As the traditional energy storage, state-of-art Lithium-Ion battery (LIB) underwent approximately 30-years investigation from firstly demonstrated by Murphy et al. [1] at the end of the 1980s. However, the relatively mature technology of LIB gradually becomes unqualified for long-range EVs and cost-efficient energy storage system [2] due to its limited theoretical energy density and expensive raw materials. This leads to an urgent exploration of next-generation cells, such as Lithium-Sulfur Battery (LSB). It possesses competitive strength in future battery market since its theoretical energy density and specific capacity reach 2600 Wh/kg and 1672 mAh/g respectively, which are several times higher than traditional LIB [3]. Meanwhile, the sulfur element is abundant and cost-efficient [4]. Furthermore, the operating voltage of LSB, 2.15 V, is relatively low compared to other traditional batteries, which reduces the possibility of operational safety issue [5] and suits for low voltage devices [6]. This thesis report will focus on the development of LSB.

1.2 Motivation

Although LSB owns outstanding theoretical behaviours, it is prevented from commercialisation mainly due to two reasons. The first one is the low electrical conductivity of sulfur, which impedes electrochemical reaction within the cathode [5]. To reduce the internal electronic resistance, a highly conductive material and binder are added, but this consequently reduces the sulfur loading, which compromises the LSB theoretical energy density. The second factor is polysulfide (PS) shuttle effect. This phenomenon occurs in the lithiation process and induces malfunction of active material – sulfur, which degrades LSB's performance in term of fast fading rate, low coulombic efficiency, and high self-discharge rate [7].

Binder plays an essential role in enhancing the capability of LSB through its binding function to mix sulfur and conductive material together in the cathode. As the conventional binder widely used in LSB, polyvinylidene fluoride (PVDF) could not deliver sufficient adhesion strength between the positive electrode and current collector [8]. This shortage turns out a larger proportion of binder in the cathode. The PVDF's characteristic of insolubility in water also requires hazardous chemical N-Methyl-2-pyrrolidone (NMP) to dissolve during cathode construction process.

In contrast, natural polymer carrageenan could substitute the commonly used binder, PVDF.

Carrageenan possesses desirable features for a binder, including water solubility, strong adhesive strength and environmental friendliness [4]. At the same time, carrageenan is capable of limit PS redox shuttle reaction through its variable sulfate leaving group, based on nucleophilic substitution reaction theory, to trap PS generated during discharging [4]. The motivation behind this thesis project is to improve LSB performance by primarily investigating on carrageenan binder.

1.3 Objectives

This section illustrates achievements completed in the overall thesis project. The uppermost objective is to advance the capability of carrageenan binder in LSB by investigating different condition might affect its performance. Main deliverables achieved during this investigation are listed below.

- Comprehensive literature reviews about LSB and its challenges;
- Identification of factors affecting the adhesion strength of carrageenan binder (including the heating temperature of binder solution, the viscosity of binder solution, the proportion of binder in cathode); and
- Comparison of batteries with carrageenan and PVDF binder through OCV, EIS and cycling test,

1.4 Scope

There are numerous factors would affect the electrochemical performance of LSB. This thesis project would only investigate the influence of binder while remaining other materials and processes constant. Table 1 would present elements in and out of scope.

Table 1 In and Out of Scope Elements

In Scope	Out of Scope
Type of binder	Impact of the proportion of Super P
The proportion of binder in the cathode	Type of active material composite
Heating temperature and concentration of binder solution	Material of anode, electrolyte, current collector, separator and casing
Relationship between thickness and sulfur loading of cathode	Electrolyte volume
Battery performance on OCV, EIS and cycling	Cycling C rate

2 Literature Review

This section will elaborate literatures related to lithium sulfur battery including its fundamental components, the working principle and major challenges encountered as well as correlated solutions. The binder component would be concentrated in this review with research on PVDF, other water-soluble binder and carrageenan.

2.1 Battery Component

The major components in battery include positively and negatively charged dual terminals (anode and cathode), electrolyte, separator and the current collector. These components will be elaborated in the following sections and a general schematic diagram of LSB is shown in Figure 1.

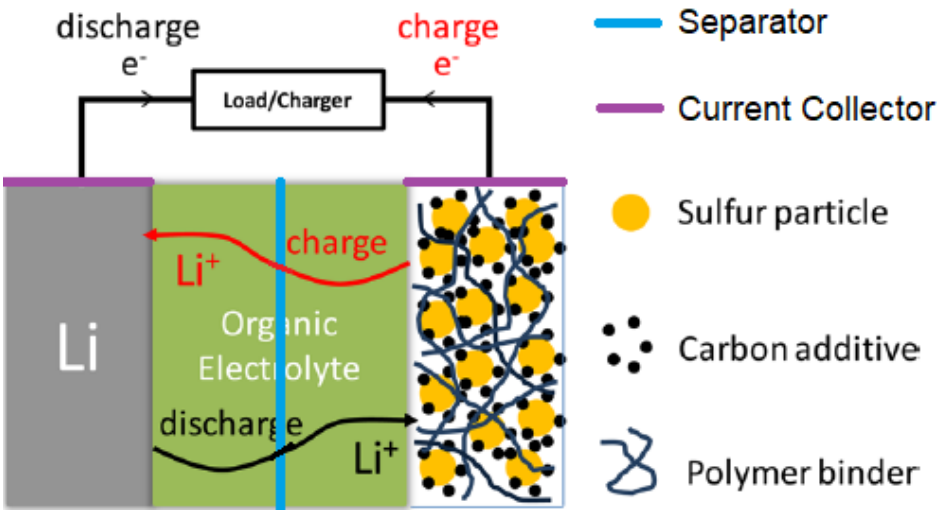

Figure 1 Schematic Diagram for LSB [5]

2.1.1 Anode

The anode, which is a positively charged electrode, contributes electrons to the cathode in charging-discharging cycles. The theoretical specific capacity of the battery is partially dependent on the material of the anode. The commonly used anode in LSB is pure lithium metal and lithium anode will be adopted in this experiment. As the lightest metal element in the world, metallic lithium owns the specific capacity of 3862 mAh/g and has been proposed as a competitive material for battery's anode [9]. Its highly reactive and flammable properties, however, increase manufacturing cost and safety risk.

Other metallic materials have also been considered into candidates for battery's anode. Aurbach's group has reported the first secondary battery with magnesium (Mg) foil as anode [10]. Compared to lithium anode, Mg would not form dendrite during electrodeposition, which makes this specific battery system safer during operation [11]. Incompatibility between anode and electrolyte, on the other hand, hinders Mg battery from practical applications [12]. Another

metallic material successfully utilized in the battery system is zinc (Zn). With high specific energy of 1086 Wh/kg, Zn-air batteries take advantage of unlimited oxygen supply in air, yet still have the problem of dendrite formation similar to lithium anode [12].

2.1.2 Electrolyte

The electrolyte in battery serves as a bridge that allows the internal transformation of ions between anode and cathode. It is composed of solvent and lithium salt, which has chemical compatibility with PS generated during cycling. Since PS anions and anionic PS radicals are highly reactive, common electrolyte solvents, like esters, phosphate and carbonates, would unfavorably participate in a chemical reaction with them [13]. To avoid such unacceptable reaction, frequently used electrolyte solvent in LSB adopts a combination of two solvents, dimethyl ether (DME) and 1,3-dioxolane (DOL), with a ratio of 1:1 [7]. This configuration of solvent with the salt of 1 M LiTFSI and 0.2 M $LiNO_3$ would be formed into the electrolyte and consistently used in LSB of this thesis project.

Meanwhile, Aurbach's team had demonstrated that the 1,3-dioxolane performed a unique function, which shapes lithium deposition into flat flakes rather than dendrites, in Li metal battery [14]. The flake-shaped lithium can readily attach to Li anode bulk and simultaneously create effective passivation films on lithium anode [14]. This type of passivated film is called solid electrolyte interface, which would prevent anode surface from the growth of dendrite during cycling [15].

This liquid electrolyte mixture would induce the PS migration in the cell because of high-order PS's solubility in the solvent, but this dissolution results in exposure of residual sulfur to the conductive material and facilitate the cycling performance of lithium/sulfur cell [7]. Even the active material in cathode possesses carbon to increase electrical conductivity, the bulk of sulfur could only be adequately utilized with the existence of PS's dissolution [7].

The relative mass ratio between liquid electrolyte and sulfur would affect specific capacity and cycling stability of LSB. Low E/S ratio degrades the utilization of sulfur electrode especially with high sulfur loading at intensive current densities [16]. This phenomenon was explained by Ding's team that lower E/S ratio renders higher PS concentration in the electrolyte and more viscous solution, resulting in inferior ionic conductivity and power capability [17]. At the same time, the lower the E/S ratio the faster the capacity retention of LSB would decay [16].

2.1.3 Separator

The separator also plays an essential role in the battery. Through its porous structure that allows permeation of metal ions yet hinders the shortcut for electrons, separator balances charges in

electrolytes, ensuring the continuity of electrochemical reaction, and prevents the battery from the danger of short circuit [18, 19]. Application of polymeric membrane overwhelms other two types of separators - nonwoven mats and ceramic enhanced membranes- in the battery due to its relatively thin thickness and friendly cost [20]. An effective separator should retain predominant mechanical properties simultaneously to withstand deformation and penetration [21].

The most conventional separator used in lithium battery is microporous polyolefin-based membranes [22]. This type of separator is stable during chemical reaction occurred in cells, and its suitable thickness could also withstand moderate mechanical force [23]. Nevertheless, its drawback of low thermal stability would lead to the safety issue since it is incapability of working under high temperature [23].

2.1.4 Cathode

In contrast, the cathode is a negatively charged electrode as an electron receiver during the reduction process. The structural morphology of cathode material would affect the electrochemical performance of cells [24]. Active material, electronic conductor and binder are three major contents that constitute the cathode and are elaborated below. Content related to carrageenan binder will be illustrated under a new section.

2.1.4.1 Active Material and Electronic Conductor

The maximum theoretical energy density is achieved when the entire cathode is made of the sulfur element, which unfortunately is impossible due to electrically and ionically insulating properties of sulfur element [25]. To compensate that drawback of active material, the electronic conductor would mix with sulfur to increase its electrical conductivity. Other than improving the electrical conductivity in cathode facilitating the utilization of active material, electronic conductor provides accommodation for around 80% volume expansion, due to the reduction of cyclic S_8 to lithium polysulfide, through its nature of high porosity and the flexibility [26]. Although the additional carbon content curtails the sulfur loading in the cathode, resulting in less energy density of cell, it contributes to increment of battery cycle life and capacity retention of sulfur [7].

The predominantly used additive in the sulfur cathode is carbon nanotube (CNT), which is sp^2-bonded carbon atoms formed into cylindrical graphene sheets [27] as shown in Figure 2 (a). The low resistance of CNT, varied from 0.34×10^{-4} to 1.0×10^{-4} ohm·cm [28], results from its chemical structure, where each carbon atom covalently bonds with three adjacent carbons and one remaining electron is unrestricted to be delocalized [27]. Jin's team stated that porosity of CNT can also encapsulate PS to some extent, which restricts the PS migration effect [26].

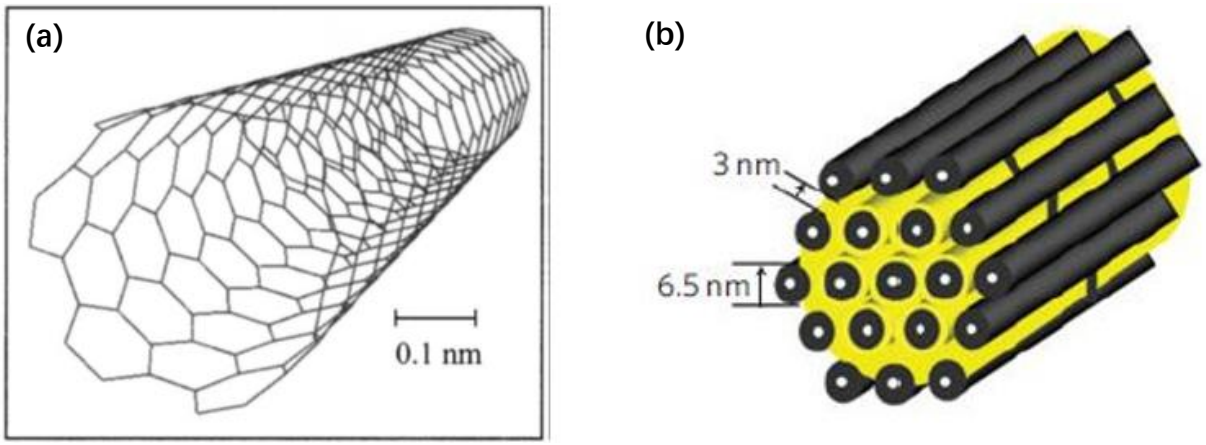

Figure 2 (a) Single-walled Carbon Nanotube [29] (b) Schematic Diagram of CMK-3 with Confined Sulfur (Yellow) [30]

Another type of conductor used in LSB is CMK-3, classified as mesoporous carbon, by Nazar's team. This highly ordered carbon matrix is composed of interconnected cylindrical mesoporous tubes in hexagonal arrangement with uniform pore diameter [31] as shown in Figure 2 (b). Nazar's team fabricated LSB with CMK-3 as the carbon framework coated with polymer on the composite to further control PS effect, which owns the specific capacity of 1,320 mAh/g [30].

In this experiment, the active material composite adopted is made from CNT60 (60 wt% sulfur and 40 wt% CNT) and Super P (SP). SP similarly provides the enhancement of electrical conductivity by percolation mechanism.

2.1.4.2 Conventional Binder

The binder plays an essential role in LSB. The primary functions of the binder are to combine various components together uniformly and to ensure excellent electrical connectivity within the cathode, while the binder is exposed to cyclic mechanical stress due to volume change of active material simultaneously [32]. The ideal binder, therefore, needs to maintain structural integrity for the lifetime of the battery during the electrochemical process. Meanwhile, to satisfy the expectation of utilizing LSB in cost-efficient transportation application, the sulfur loading of more than 7 mg/cm^2 is required [33]. The cathode layer, however, tends to form cracks and even peel off from the current collector when the sulfur loading gets higher, i.e. thicker electrode layer [34]. Thus, a specific binder with strongly cohesive strength is demanded to achieve high sulfur-loading cathode. Otherwise, a poor binder will have a direct impact on the battery performance by reducing cycling stability of the cathode [35].

2.1.4.2.1 PVDF

The conventional binder, PVDF, shows good performance in LIB for its high conductivity and excellent resistance to the electrochemical potentials, i.e. good chemical stability [32, 36]. Lacey's team, however, states that the electrochemistry of LIBs is totally different from the

counterpart of LSBs because the chemical reaction in solution plays a crucial contributor of cycling process of the latter [37]. As such, although the PVDF has been optimized for LIBs intensively during recent decades, it may be less suitable for LSBs.

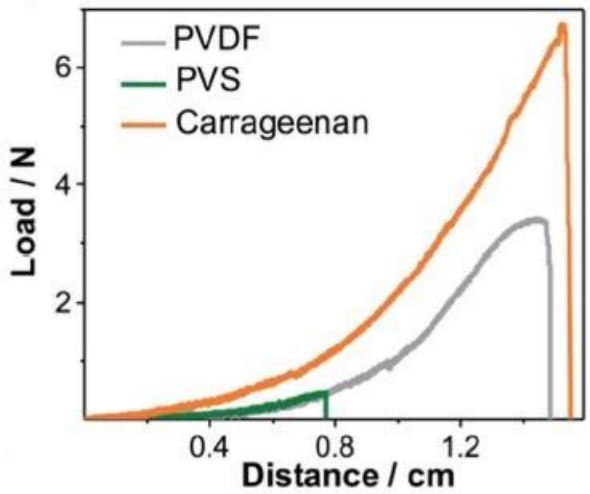

Figure 3 Adhesive Strength of Different Binders through Peel Test [4]

A shortcoming of PDVF includes insufficient adhesive strength as shown in Figure 3 when compared to Carrageenan. The low binding strength of PVDF does not allow the formation of the thick cathode to achieve higher sulfur loading. Moreover, the adoption of toxic NMP as the solvent will increase manufacturing cost as well as the damage to the environment. Another significant drawback is that PVDF will penetrate pores of CNT and dramatically block the pre-infiltrated sulfur in smaller pore from interaction with electrolyte, resulting in lower utilization rate of sulfur and faster capacity fading [38].

Meanwhile, PVDF does not show strong leaving group reactivity due to its fluoride structure, which cannot trap the polysulfide in the cycling process [39]. PVDF, hence, only generates physical a binding effect in the cathode and cannot retain active material during cycling test caused by dissolution of polysulfide in electrolyte [40].

2.1.4.2.2 Water-Soluble Binders

To avoid degradation of cell performance induced by drawbacks of using PVDF as the binder, investigations toward developing other types of binder have been made. The most prevailing type is a water-soluble binder. Polyethylene oxide (PEO) is the most prevalent one among the aqueous-processable binders and accounts for 15.9% of electrode binder used in LSB just after 43.6% PVDF [41]. This binder could alter the cathode system locally, suppress the formation of passivation on the cathode surface and motivate the redox reaction in a cell [42]. Through the covalent bonding between PEO and sulfur-carbon composite, the polymer forms a physical barrier preventing polysulfide from diffusing into the electrolyte and retards the decaying rate

[43]. However, its characteristic of crystalline–amorphous transition at 60 – 70 °C would prompt the aggregation of active material and conductor, with separation between the cathode and current collector [44]. Meanwhile, PEO exhibits swelling behavior in contact with the electrolyte, which results in larger electrical resistance and inferior cell performance.

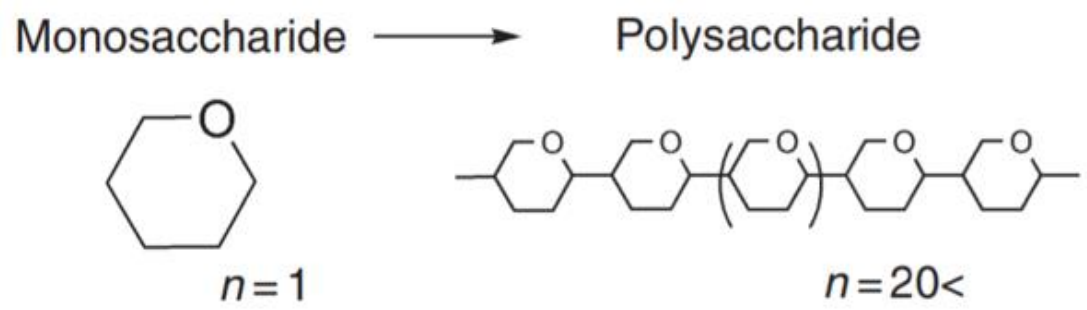

Figure 4 Chemical Structure Pattern of Polysaccharide [45]

Within the category of water-soluble binder, the polysaccharide has been chosen as other alternative solution for binder components due to its strong mechanical strength. The polysaccharide is composed of more than 20 monosaccharides linked with glycosides as shown in Figure 4 [45]. The long-chain molecule could easily bind active material and electrical conductor together. Beside some commonly used polysaccharides binders, like carboxymethyl cellulose (CMC), Liu's team reported a novel material for the binder that weaves two polysaccharides together to form robust networks, which is capable of retaining ultrahigh sulfur loading of 19.8 mg/cm^2 [46]. With sufficient oxygen-containing functional group, the combination of guar gum (GG) and xanthan gum (XG) has been shown to favour the formation of interaction site to bind PS.

Another potential polysaccharide-based biopolymer as binder is guar gum (GG), extracted from guar beans. Cheng's team [47] concluded that retrograded GG promotes the homogenous dispersion of compositions in the cathode, resulting in better electrochemistry. The retrogradation will cause reaggregation of GG molecule in solution and then increase the fluidity along with time [47]. This work experiment inspired a new investigation direction, that whether carrageenan binder solution possesses retrogradation property and whether the retrogradation of carrageenan affects the performance of LSB.

The aqueous-processable binder, including abovementioned examples, is generally abundant, cost-efficient and eco-friendly. With water as the solvent, this type of binder can avoid utilization of organic solvent, which is toxic and harmful to the environment. Meanwhile, the inherent hydroxyl groups within the water-soluble binder show affinity to the aluminum foil with the hydrophilic oxide surface layer, resulting in stronger adhesion [48].

2.1.5 Carrageenan

Carrageenan is another polysaccharide-based biopolymer extracted from red seaweeds, which is primarily used in food industries for gelling and thickening purposes [2]. Unlike other common polysaccharide binders, the repetitive chemical structure of carrageenan is a disaccharide unit, which is composed of D-galactose and 3,6-anhydro-galactose (3,6-AG) as backbone [49]. Meanwhile, carrageenan can be categorized into three main types, i.e. lambda, kappa and iota, based on different content and position of ester sulfate and content of 3,6-AG [2]. However, only kappa and iota carrageenan (kCar and iCar) are considered as binders in this thesis project and their general repetitive chemical structures are shown in Figure 5 with identifications of ester sulfate, D-galactose and 3,6-AG.

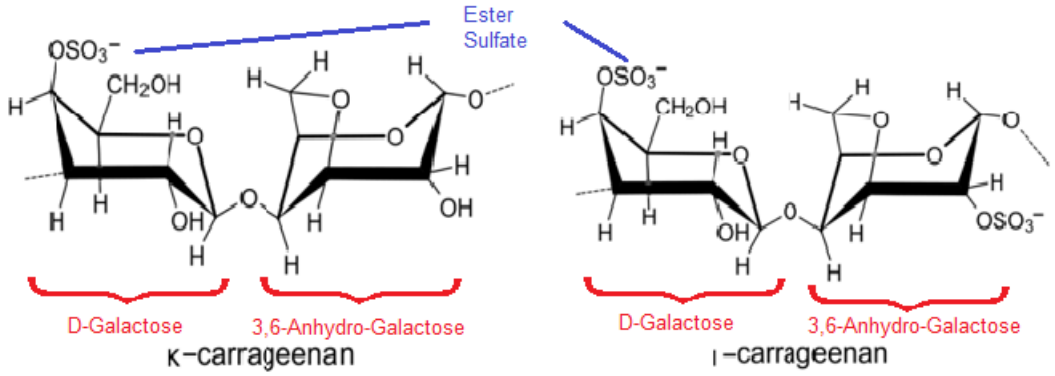

Figure 5 Chemical Structure of kCar and iCar [2]

2.1.5.1 Properties of Carrageenan

Since the chemical structures of iCar and kCar are distinctive to each other, their chemical and physical properties also show differences. The chemical reactivity of carrageenan is predominantly determined by its strongly anionic ester sulfate group [2]. Meanwhile, the ester sulfate group in carrageenan has a strong polarization feature, which makes it an ideal leaving group for nucleophilic substitution reaction with polysulfide without introducing new species into the system [4]. The existence of ester sulfate group would also influence the solubility properties. The higher composition of hydrophilic ester sulfate and hydroxyl group in carrageenan, the larger solubility it will have, while the content of hydrophobic 3,6-AG would degrade the solubility on the other hand [50]. With 32% of ester sulfate and 26% of 3,6-AG approximately, iCar has a higher solubility in water than kCar, which has 22% and 33% content of ester sulfate and 3,6-AG, respectively [49]. The soluble temperature, nevertheless, of both carrageenan is above 60 °C [50]. Meanwhile, the viscosity of carrageenan solutions increases exponentially with concentration and decreases with temperature.

2.1.5.2 Gelling Properties of Carrageenan

A higher level of ester sulfate in iCar also reduces gel strength and makes the gel more elastic

and cohesive, while the kCar generates stronger and more brittle gel structure [50]. The gelation is formed when random coils of polysaccharide at high temperature transfer to helical shapes when cooled down [51]as shown in Figure 6 and this process is thermally reversible.

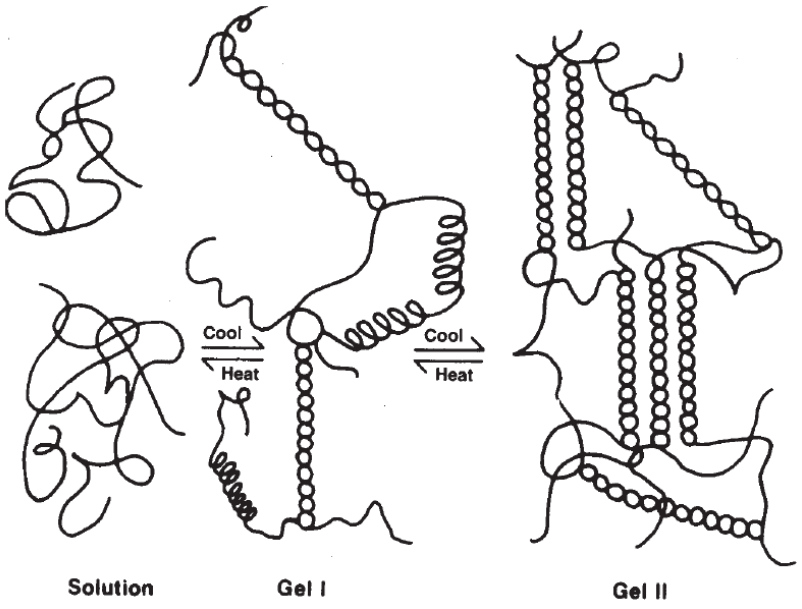

Figure 6 Gelling Mechanism [50]

Elastic iCar is only cooled to Gel I stage with relative loose gel, while kCar forms into Gel II stage with a more rigid structure. Moreover, the presence of other ions in solution would facilitate the formation of water gel. Potassium ion would promote the gelation of kCar even the concentration of kCar in water is only 0.5% and calcium ion would promote the gel formation of iCar [2]. Those ions tend to form bridges between adjacent helices by bonding with sulfate groups, thereby facilitates gelation even when there is no enough carrageenan to bind together by itself [50].

2.1.5.3 Carrageenan as Binder in LSB

Up to now, only Ling's group reported their work of using lambda carrageenan as cathode binder in LSB system. The presence of the ester-sulfate group (OSO_3^-) and several hydroxyl groups increases the hydrophilia of carrageenan and allows it to be soluble in water above 60 °C [50]. Meanwhile, carrageenan possesses stronger adhesive strength than PVDF [4], resulting in a higher sulfur-loading and consequently a larger specific battery. Another benefit is that carrageenan has stable sulfate leaving groups, which could fix shuttling polysulfide on cathode via C-S covalent bond based on nucleophilic substitution reaction [4]. This direct grafting of the polysulfide onto the binder provides a close connection with the conductive network. This means it can readily receive electrons for electrochemical reactions, reducing charge transfer impedance.

Ling's team adopted ratio of sulfur to binder of 5:1 for their battery and achieved 17.0 mg/cm2 sulfur loading with initial discharging capacity of 1199.1 mAh/g at 0.01 C [4]. Meanwhile, this ratio is calculated to trap as many polysulfides as possible while not compromise energy capacity and only caused 1.5 wt% irreversible capacity loss due to C-S covalent bond [4].

2.1.5.4 Other Applications of Carrageenan in Battery

Besides the application of binder in LSB, carrageenan also has been investigated for other purposes in battery by different teams. Cuesta et al. employed seven different hydrocolloids as binder in lithium-ion battery including carrageenan [52]. However, carrageenan has been demonstrated as poor electrochemical performance compared to other hydrocolloids due to its relatively low cohesive strength and gelling properties [52]. Since the electrochemical reactions within LSB and LIB are different, the function of carrageenan used as the binder in LIB is merely providing mechanical cohesive strength to bind active material together without the occurrence of any chemical reaction.

The application as a solid electrolyte in the battery has been investigated by Camacho's team with a focus on kappa carrageenan [53] and by Moniha's group with a focus on iota carrageenan [54]. With cost-efficient and environmentally-friendly features, biopolymer, carrageenan, is promising to replace the conventional synthetic polymer used in cells [54]. Meanwhile, carrageenan-based electrolyte demonstrated higher conductivity compared to other biopolymers with 3.25 ×10-4 S/cm for kCar and 3.25 ×10-3 S/cm for iCar [53, 54]. The conductivity is influenced by temperature, where the increased temperature would enhance the mobility of ions in the polymer chain, resulting in increased ionic conductivity [55].

2.2 LSB Working Principle

The basic electrochemical reaction of LSB during discharging and charging process will illustrate in this section. The voltage profile of LSB with corresponding chemical elements is shown in Figure 7.

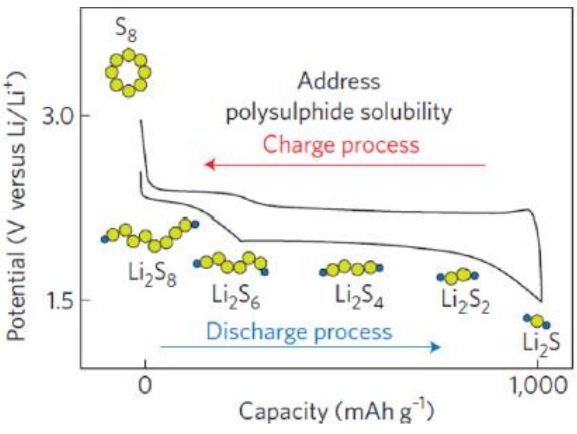

Figure 7 Voltage Profile of LSB [56]

The electrochemical operation of the cell starts with discharging since octa-sulfur (S_8) is in the charged state initially. When anode and cathode are connected with an external circuit, lithium metal in the anode is oxidized and forms electrons and lithium ions. Electrons move toward cathode via an external circuit, while lithium ions penetrate separator via electrolyte to join the reduction in the cathode. S_8 is then reduced to Li_2S_8 by accepting the electrons and lithium ions from the anode. The voltage also drops from 2.65 V to around 2.2-2.3 V, which shows the first discharging plateau, since the cell potential of Li_2S_8 is lower than sulfur element. The chemical equations of oxidation and reduction process are shown in Equation 1 and 2.

$$2Li \rightarrow 2Li^+ + 2e^- \quad (1)$$

$$S_8 + 2Li^+ + 2e^- \rightarrow Li_2S_8 \quad (2)$$

Along with the continuous oxidation in the anode, Li_2S_8 solution is further reduced to less soluble Li_2S_6 and Li_2S_4 with a voltage drop to 1.9-2.1 V, where is the second discharging plateau and the major contributor of energy capacity. Equation 3 and 4 illustrate their reduction process.

$$3Li_2S_8 + 2Li^+ + 2e^- \rightarrow 4Li_2S_6 \quad (3)$$

$$2Li_2S_6 + 2Li^+ + 2e^- \rightarrow 3Li_2S_4 \quad (4)$$

Eventually, Li_2S_4 solution converts to Li_2S_2 and Li_2S solid in the cathode, which reaches the maximum capacity of a battery without further discharging. Since the insoluble and non-conductive nature of Li_2S_2 and Li_2S, voltage potential drops again due to high polarization [7]. Equation 5 and 6 are listed below to show the final reduction of polysulfide.

$$Li_2S_4 + 2Li^+ + 2e^- \rightarrow 2Li_2S_2 \quad (5)$$

$$Li_2S_2 + 2Li^+ + 2e^- \rightarrow 2Li_2S \quad (6)$$

$$8Li_2S \rightarrow 16Li + S_8 \quad (7)$$

The Equation 7 summarizes charging process, where Li_2S converts back to S_8 via formation of gradually increased lithium polysulfide, creating a reversible cell cycle [57].

2.3 Challenges of LSB

There are several challenges inherited in cell chemistry of LSB and hindered it from commercialization. This section will describe some significant challenges and their corresponding solutions from current investigations.

2.3.1 Low Conductivity and Volume Expansion of Sulfur

As the active material in cathode, sulfur elements and the intermediate polysulfides created

during the lithiation process have low electrical conductivity, around 5E-30 S/cm [58]. Although the Gibbs energy of the reaction between lithium and sulfur is enormous, the low conductivity will cause erratic electrochemical contact within battery cathode and diffusion of ions and electrons on the surface merely. At the same time, the reaction of converting S_8 to Li_2S would ultimately cause a volumetric increment by 79.2%, which induces internal strain along with pulverization in cathode and loss of contact between the electrode and current collector [59].

The basic solution to address these properties of sulfur is mixing high-conductivity and porous additives with sulfur. Porous carbon material has undergone intensive development to perform such function, including the CNT and SP used in this experiment. According to the different size of pores, the carbon material can be classified into microporous carbon, mesoporous carbon, macroporous carbon [59]. The microporous carbon has been found that it is adequate to transfer electrons because of high electrical conductivity and immobilize the sulfur element and polysulfide due to tiny pores [60]. Based on the experiment done by Ryu's group, however, the small pore size hinders the contact between sulfur and electrolyte, resulting in insufficient transport of Li ions, and leaves limit volume to adopt volume variation [61].

To further retain the polysulfide within the additives and accommodate the volume expansion, a novel morpho of yolk-shell structure has been prepared and investigated by Zhou's group [62]. By heating the polyaniline−sulfur core−shell structure, polyaniline shell is vulcanized along with shrinkage of inner bulk sulfur, causing void space in between [62]. The entire fabricating process is shown in Figure 8. The high-conductivity of polyaniline shell and sufficient space for sulfur expansion result in better electrochemical performance than core-shell structure, with 1100 mAh/g specific capacity and 70% retention after 200 cycles at 0.2 C [62].

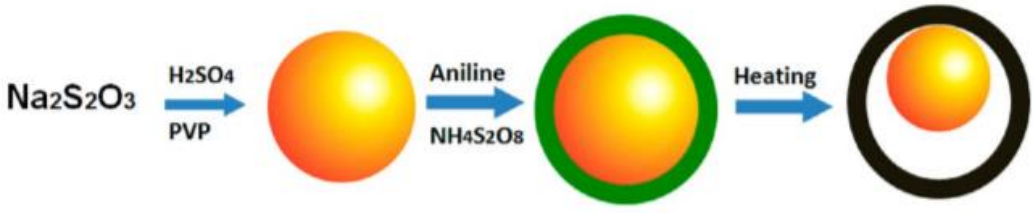

Figure 8 Synthesis of Yolk-Shell Structure [62]

2.3.2 PS Shuttle Effect

Polysulfide shuttling effect is the thorniest challenge occurred in LSB, causing detriment in cell performance with low coulombic efficiency and rapid self-discharge rate [7]. The following

figure shows the general mechanism behind PS redox shuttle.

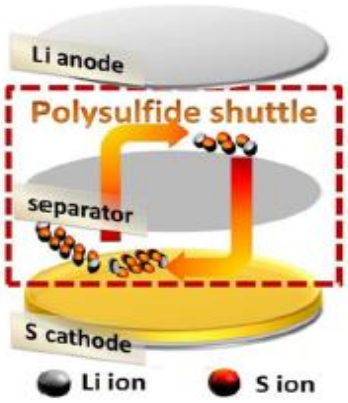

Figure 9 Polysulfide Redox Shuttle Effect in LSB [5]

During the lithiation process in the cathode, various high-order polysulfides (Li_2S_n, 6<n≤8) are generated and soluble in a liquid electrolyte, a mixture of DME and DOL; thus, the lithium polysulfide could traverse separator and migrate between lithium anode and sulfur cathode. Partial high-order polysulfide would collect electrons directly from the anode and be reduced to insoluble and insulating low-order polysulfide (Li_2S_n, n=1,2), which deposits on the anode and inaccessible to the cathode, causing irreversible loss of active material [56]. The PS shuttling rate is determined by the structure of the positive electrode, the solubility of PS in electrolyte and migration characteristic of the electrolyte system [63].

There are many solutions that can mitigate or eliminate the PS redox shuttle effect. One intensively focused method is utilizing additives to physically trap the PS and slow down its propagation speed. These carbon materials contain amorphous carbon, carbon nanofibers, expanded graphite, graphene oxide and etc. [6]. Xin's team [23] synthesized small sulfur molecules of S_n (n=2-4), which can be confined in porous carbon matrix and avoid the formation of soluble polysulfide. Due to the open-ended structure of porous carbon, polysulfide could still leak to the electrolyte to some extent, which makes a physical reservation an ineffective method.

Another solution is to form chemical bonds between high-order polysulfide and polymer conducting agent or binder, just like ester sulfate group of carrageenan. Conducting polymer, like Polyaniline (PAN), polypyrrole (PPY), and polythiophene (PT), owns doped protons, which link the polymer with polysulfide via H-bonds. Polymer binder, such as gelatin, polyethylene oxide, carbonyl-β-cyclodextrin, etc., concurrently forms a lithium-oxygen bond due to the existence of carbonyl groups [2].

Other than solutions related to cathode components, there are also many efforts dedicated

toward the development of separator part to alleviate PS shuttle effect. Freitag's team reported a novel separator material, which incorporates polyvinylsulfate potassium salt (PVSK) into the membrane of polyvinylidene fluoride-hexafluoropropylene (PVdF-HFP) [64]. The PVSK additives could physically block the porosity within separator as well as electrostatically repulse the negatively charged polysulfides away from the separate, presenting negligible capacity decay [64]. Meanwhile, by inserting an interlayer between separator and cathode can also impede the migration of polysulfide [34]. One of the adequate approaches is a mixture of titanium oxide (TiO_2) nanoparticles and carbon nanofibers constructed by Zhao's group [65]. TiO_2 acts as an anchor to trap polysulfide chemically while the carbon nanofiber provides reaction sites for TiO_2 and polysulfide and also mechanical strength to support TiO_2 [65].

2.3.3 Dendrite Formation in Anode

The major problem existed in anode composed of lithium is dendrite formation, arising from the instability of solid electrolyte interphase layer (SEI layer) [57]. This unstable SEI layer is generated by a reaction between lithium and electrolyte and protects lithium from further reaction [66]. Electrodeposited lithium shapes into dendritic morphology during charging process since SEI is incapable of uniformly arranging the commuting lithium ion [67] as shown in Figure 10. Li dendrites structure probably will penetrate the separator, causing internal short-circuit [68] and fast capacity fading [67].

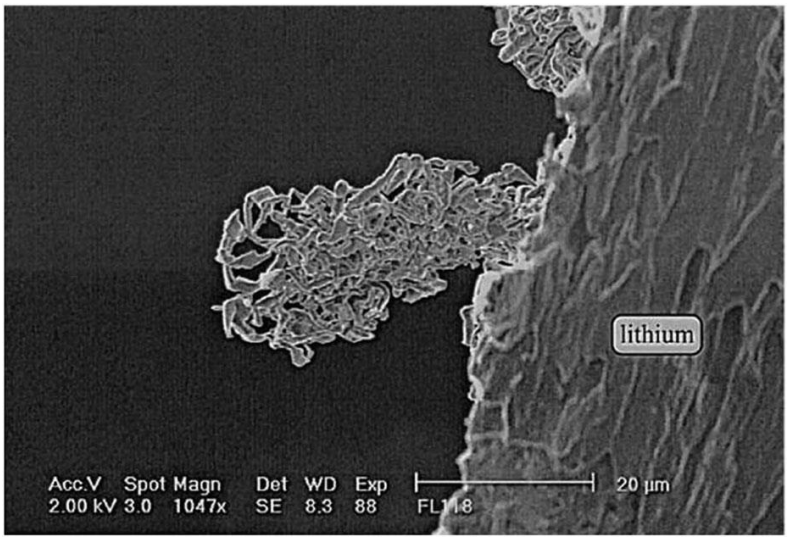

Figure 10 Dendritic Li Formation [69]

To alleviate this problem, Lee's team [6] introduced a protection layer coated on lithium anode surface as a physical barrier to suppress the formation of SEI layer. The protection layer is made of curable monomer (polyethylene glycol dimethacrylate) with the occurrence of liquid electrolyte and photoinitiator, through UV curing method [6]. This method resulted in lower initial electrical capacity compared to the unprotected cell due to higher internal impedance but

demonstrated more stable electrochemical performance with effective retention of capacity after 100 cycles [6].

Except preventing the growth of lithium solid electrolyte interphase layer directly, a uniform arrangement of commuting lithium ion could also avoid the formation of dendrites. With the utilization of PEO-ceramic gel electrolyte, Mikhaylik's team constructed a battery with slower decaying rate and safer operational conditions [70]. This electrolyte possesses sticky property to hold the separator and lithium anode together and generate favorable lithium deposition in between rather than dangerous dendrites [7].

3 Experimental

This section will illustrate entire procedures of material preparation for this thesis project, including producing binder solutions and active material, synthesizing cathodes and constructing batteries. Meanwhile, all testing methods are elaborated in this section as well.

3.1 Material Preparation and Battery Construction

3.1.1 The Binder Solution

The binder solutions were produced by mixing carrageenan powder and distilled water together. Firstly, purified iCar and kCar (purchased from Sigma-Aldrich initially and bought new powder from Melbourne Food Depot after the first batch of powder was used up) powder were weighted accordingly and added into the beaker with 20 ml distilled water. The mixtures were then placed on a continuously-heated hotplate and stirred for 60 minutes with a magnetic stirrer. Different heating temperature and concentrations of solution were also prepared to investigate factors that influence the adhesive strength. All binder solutions were prepared based on Table 2.

Table 2 Different Conditions of Carrageenan Solutions

Binder Solution #	Carrageenan Type	Carrageenan Mass (mg)	Concentration (wt%)	Heating T (°C)
1	iCar	40	0.2	80
2	iCar	540	2.7	80
3	kCar	40	0.2	80
4	kCar	540	2.7	80
5	iCar	40	0.2	40
6	kCar	200	1	80
7	kCar (new)	200	1	80
8	kCar (new)	100	0.5	80

3.1.2 The Active Material

The active material adopted in this experiment was CNT60, which was composed of 40 wt% CNT and 60 wt% sulfur elements (purchased from Sigma-Aldrich). At first, the CNT and sulfur were weighted and then mixed with mortar and pestle. After mixing was completed, the CNT60 mixture was sealed in a glass tube and then placed into an autoclave. The autoclave was subsequently transferred to the oven for 24-hour heating at 160 °C. During this process, the sulfur element would melt into the porous structure of CNT.

3.1.3 The Cathode

Two types of cathode were fabricated; one was the PVDF-based cathode and the other was with the carrageenan binder. Both cathodes were composed of the CNT60, Super P (purchased from Sigma-Aldrich) and binder. These materials were first weighted and then mixed with a mortar and pestle until a homogeneous slurry was obtained. Subsequently, the slurry was transferred

to the carbon-coated aluminum foil (CCAF) for the PVDF-based cathode and the aluminum foil (AF) for the carrageenan-based cathode. An adjustable blade was then used to deposit the slurry layer with uniform thickness on the current collector foil. Thicknesses of loading gap were set at 350 μm and 600 μm for CCAF and AF respectively. The sample was placed into a vacuum oven for 12-hour drying at 60 °C. After drying, the cathode was cut into rounded discs via a metal puncher.

The proportion of CNT60 would decidedly influence the sulfur loading in the cathode. The cathode slurry weight ratio of PVDF-based cathodes and carrageenan-based cathode was 8.825:1:0.175 or 8.5:1:0.5 or 8:1:1 for CNT60, SP and bulk of PVDF or carrageenan binder respectively. The initial composition of 8.825:1:0.175 in cathode was used for adhesive strength comparison between two binders, while cathodes of later two ratios were constructed into batteries for testing. Since the cathodes with new kCar showed major inhomogeneity and poor adherence as proven in section 4.1.2.3, only iCar and PVDF binder were used to fabricate cathodes. Thus, the testing matrix of cells was constructed to compare performance between iCar and PVDF with cathodes possessing the following compositions (active material: additive: binder), as shown in Table 3.

Table 3 Testing Matrix

Cathode Type	5 wt% iCar	10 wt% iCar	5 wt% PVDF	10 wt% PVDF
Composition (Active Material: Carbon Additive: Binder)	85:10:5	80:10:10	85:10:5	80:10:10
Active Material (mass)	CNT60 (85 mg)	CNT60 (80 mg)	CNT60 (85 mg)	CNT60 (80 mg)
Carbon Additive (mass)	SP (10 mg)	SP (10 mg)	SP (10 mg)	SP (10 mg)
Binder (mass)	iCar (5 mg)	iCar (10 mg)	PVDF (5 mg)	PVDF (10 mg)

3.1.4 The Battery

The entire procedures of assembling batteries were conducted in the glovebox (MBRAUN UNIlab). The anode side case was placed upside down on the workbench and followed by cone spring and spacer. The pure lithium metal was then put on the spacer. The electrolyte used in the battery was 1 M LiTFSI and 0.2 M LiNO3 in DOL/DME solvent and the amount of electrolyte adopted was 20 μl/mg of a bulk mass of sulfur in the cathode. After adding half amount of electrolyte on the lithium anode with a pipette, the separator was laid on the electrolyte to get saturated and cover the anode. Subsequently, the other half amount of electrolyte was dropped on the separator and the cathode was then placed on the top with the

side of active material attached to the electrolyte. After capped by the bottom case, the battery was transferred to hydraulic compressor for final compression. All components expect lithium anode, electrolyte and cathode are shown in Figure 11 according to the order of assembly.

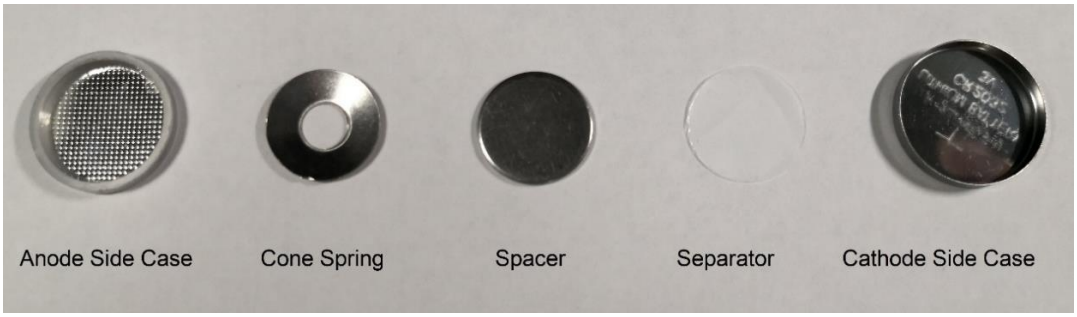

Figure 11 Battery Components in Assembling Order

3.2 Binder Solution and Cathode Testing

3.2.1 The Viscosity of Carrageenan Solution

To determine the change of viscosity of carrageenan binder solution along with time, the container of the solution was fixed on the workbench for snapshots just after production, day 2, 3 and 7. These photos were then combined for comparison. The slope of inclined binder solution can indicate the viscosity indirectly and variation of slope within one week can be used to determine whether the viscosity of the solution is time-dependent.

3.2.2 Sulfur Loading and Thickness

The mass of produced cathodes was measured by a scale and used for calculation of the mass of bulk sulfur and sulfur loading based on equation 8 and 9.

$$Mass\ of\ Sulfur = \left(m_t - m_{foil}\right) * \%_{am} * \%_{cathode} \tag{8}$$

$$SL = \frac{Mass\ of\ Sulfur}{\pi {r_{foil}}^2} \tag{9}$$

Where m_t is the mass of cathode coin in $[mg]$; m_{foil} is the mass of the current collector in $[mg]$; $\%_{am}$ is the weight percent of sulfur in active material; $\%_{cathode}$ is the proportion of active material in cathode; r_{foil} is the radius of the current collector in $[cm]$; and SL is the sulfur loading of cathode in $[mg/cm^2]$. The cathodes with sulfur loading around 2.5 mg/cm^2 were preferred to fabricate into batteries for comparison of cycling testing.

The thickness of the cathode is then measured by micrometer screw gauge. Since the thickness measurement might undermine the integrity of cathode, only portion of cathodes underwent this process.

3.2.3 SEM and EDS Testing

Scanning electron microscopy (SEM) generated the sample's photo and determined the

topography and composition of a sample through a focused beam of electrons to scan the surface. Through energy dispersive X-ray spectroscopy (EDS) technique, element and chemical properties of the sample could be analyzed based on the information gathered by SEM. The SEM apparatuses used in this experiment were TM3030 and SU3500 and magnification of lower and higher times were adopted for analysis.

3.3 Battery Testing

3.3.1 Open Circuit Voltage Testing

Open circuit voltage (OCV) testing was utilized in this experiment to determine the difference of electrochemical potential of two electrodes in cells without connecting to any external loads. The OCV could be calculated based on the Nernst equation shown below.

$$E_{OCV} = E^{\theta} - \frac{RT}{nF} lnQ \tag{10}$$

Where E_{OCV} is the cell potential at temperature interested in V; E^{θ} is the standard cell potential in V; R is the universal gas constant in J/K·mol; T is the temperature in K; n is the number of electrons transferred; F is the Faraday's constant C/mol; and Q is the reaction quotient of the chemical reaction in cells. But the experimental method of measuring OCV was through connecting cells to EC-lab channel and the OCV can be easily read off from the spectrum over a period. This testing method was conducted on cells before and after the cycling test to inspect the difference of electromotive force.

3.3.2 Electrochemical Impedance Spectroscopy

The electrochemical impedance spectroscopy (EIS) has been demonstrated as an effective approach to characterize the physical and electrochemical behaviors of LSB [71, 72]. In general case, the EIS could be represented in a Bode plot or a Nyquist plot and Nyquist plot had been chosen for graphics tool in this experiment. A corresponding electrical circuit was designed by Canas's team to model the EIS of lithium sulfur battery, shown in Figure 12 (a) [71]. Meanwhile, interpretations of each block were explained in an ideal Nyquist plot presented in the report of Pulido's team as shown in Figure 12 (b) [73]. R_0 represented the ohmic resistance of batteries while R_1 and R_2 stood for the resistance of solid electrolyte interface at anode side and charge transfer of sulfur intermediate respectively [71]. R_3 accounted for the resistance of S_8 and Li_2S and R_4 showed the effect of diffusion processes [71]. The sequence of resistance of all components followed on the testing frequency from high to low degrees. R_0 and R_2 would be mainly investigated in this project, which concerns more on how carrageenan binder influences the polysulfide effect.

This experiment conducted EIS testing before and after the cycling test to perceive the change

of physical and electrochemical behaviors within LSB. The batteries were connected to EC-lab equipment with frequency from 100 kHz to 100 mHz within -10 to 10 voltage range.

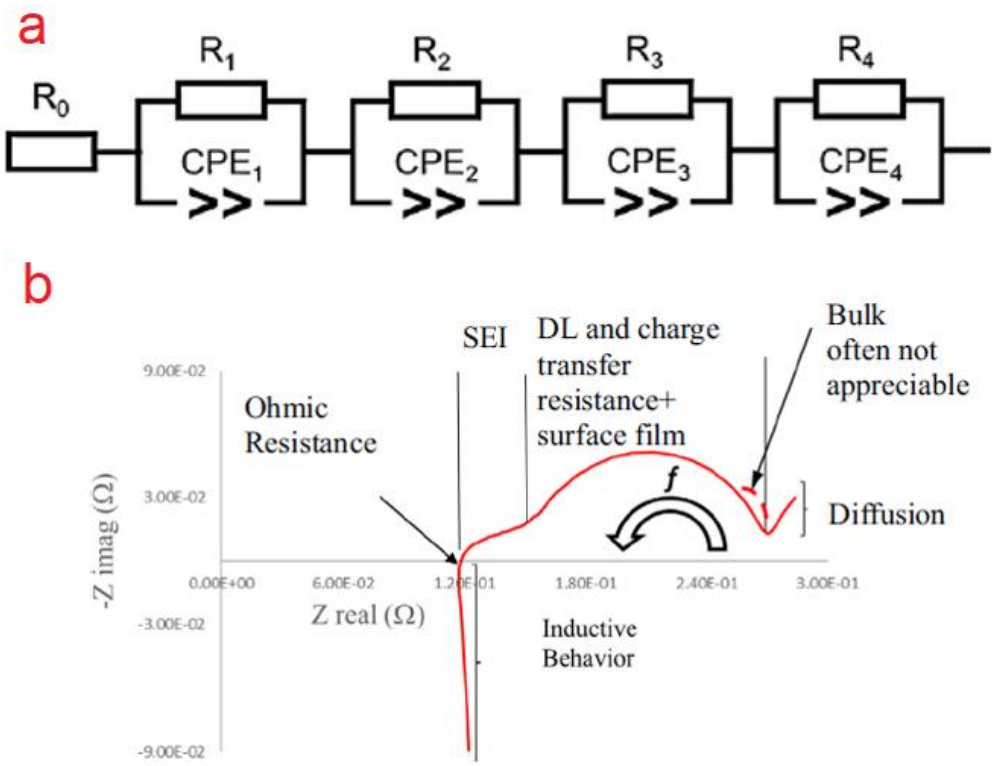

Figure 12 (a) Equivalent Electrical Circuit for EIS of LSB [71] (b) Ideal EIS in Nyquist Plot with Five Characteristics [73]

3.3.3 Cycling Testing

After OCV and EIS testing, batteries went through the cycling testing on LAND apparatus. Cycling testing is capable of inspecting many electrochemical performances of LSB, including the voltage plateaus during charging and discharging process, specific discharging capacity, coulombic efficiency and so on. The plots of specific discharging capacity against voltage profile and plots of cycling times against specific discharging capacity and coulombic efficiency would be constructed for comparisons of performance between batteries. The testing parameters are listed in Table 4.

Table 4 Cycling Testing Parameters

Parameters	Value	Unit
C Rate	0.5	C
Cycling Time	200	N/A
Charging Voltage	<=2.8	V
Discharging Voltage	>=1.7	V
Initial Resting Period	10	h

4 Results

All experimental results are presented in this section as well as thorough descriptions. It will start with the investigation of carrageenan binder solutions and corresponding cathodes. The SEM and EDS results of carrageenan powder and cathode would be presented subsequently, and battery testing results would be shown at the end of this section.

4.1 Carrageenan Binder

Since there were limited investigations about carrageenan binders in literature, this section would present some experiments about properties of carrageenan binder solutions and effects of those solutions on the cathode. All information about carrageenan binder solutions were listed in Table 2.

4.1.1 Effect of Time on Viscosity

As mentioned in section 2.1.4.2.2, retrogradation feature of aqueous GG solution gradually decreased its viscosity, which was inversely related to dispersion of constituents in cathode and cell performance [47]. Therefore, this subsection would investigate the correlation between time and viscosity of carrageenan solution. The images presented in Figure 13 were for the binder solution #1 (iCar_0.2 wt%_80°C). The images were taken just after fabrication (hot status), air cooled to room temperature (around 25 °C), and at day 2, 3 and 7.

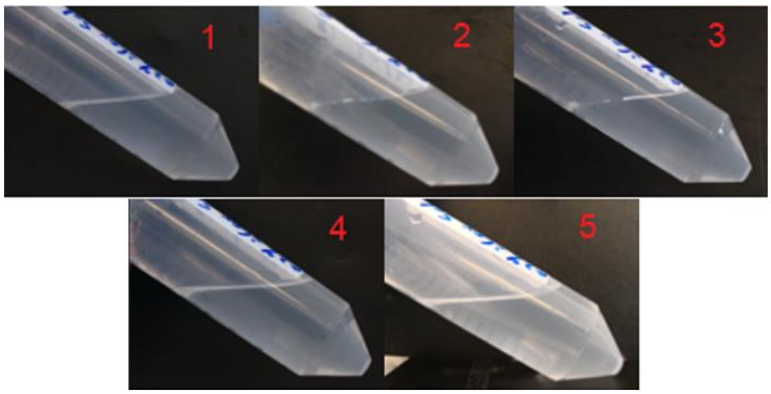

Figure 13 Binder Solution #1 (iCar_0.2%_80°C): (1) Hot Status; (2) T_{room}; (3) Day 2; (4) Day 3; (5) Day 7

The transition of viscosity was observed through the slope change of the carrageenan solution in the plastic tube. A large slope represented a higher viscosity. It was obvious that the viscosity of solution #1 (iCar_0.2wt%_80°C) was not time-dependent and the slope of the surface was approximately constant throughout the entire period. Meanwhile, there was no gelation formed in solution. However, Cheng's team utilized GG solution with 2.7% concentration while the iCar composition in binder solution #1 (iCar_0.2wt%_80°C) was only 0.2 wt%, thus might not be sufficient to distinguish the change of viscosity. Therefore, binder solution #2 (iCar_2.7wt%_80°C) was produced with higher concentration while kept other variables same

as solution #1 (iCar_0.2wt%_80°C). After the same procedures, photos of binder solution #2 (iCar_2.7wt%_80°C) were taken at the same time points and shown in Figure 14.

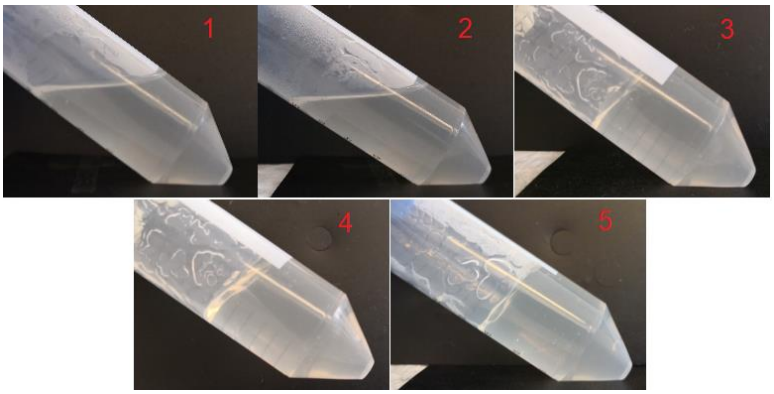

Figure 14 Binder Solution #2 (iCar_2.7wt%_80°C): (1) Hot Status; (2) T_{room}; (3) Day 2; (4) Day 3; (5) Day 7

The iCar solution with higher concentration demonstrated distinctive properties compared to the previous sample. At first, through observing the vortexes generated under the same stirring speed as shown in Figure 15, the fluidity of binder solution during the production process was less for a higher concentrated sample with deeper color. This phenomenon implied the increasing viscosity of carrageenan binder along with concentration. Secondly, the iCar solution #2 (iCar_2.7wt%_80°C) gelatinized at day 2 with an obvious gelation texture as shown in Figure 14 (3), while iCar solution #1 (iCar_0.2wt%_80°C) did not display any signs of gel. However, unlike the GG solution, the carrageenan solution does not exhibit retrogradation phenomenon without changing in slope even with increased concentration. Therefore, the viscosity of the iCar solution could not classify into time-dependent characteristic after gelation.

Figure 15 Viscosity Comparison of 0.2 wt% iCar Solution (left) and 2.7% iCar Solution (right)

The viscosity tests for binder solution #3 (kCar_0.2wt%_80°C) and #4 (kCar_2.7wt%_80°C) were also conducted to inspect whether the fluidity of kCar is time-dependent. The results shown in Figure 16 and Figure 17 proved that kCar solution did not retrograde over time and the viscosity of gelation formed in both types of carrageenan solution would not alter along with time; yet the gelation formed in solution #4 (kCar_2.7wt%_80°C) was less viscous than that in solution #2 (iCar_2.7wt%_80°C), showing a less inclined slope. This may be caused by

different properties of the gel formed by kCar.

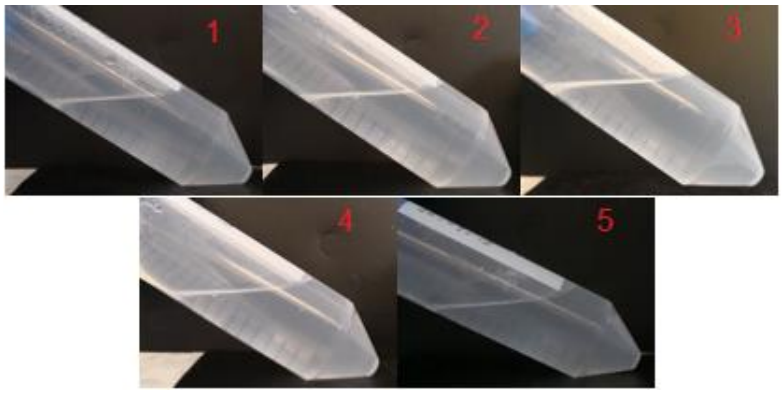

Figure 16 Binder Solution #3 (kCar_0.2wt%_80°C): (1) Hot Status; (2) T_{room}; (3) Day 2; (4) Day 3; (5) Day 7

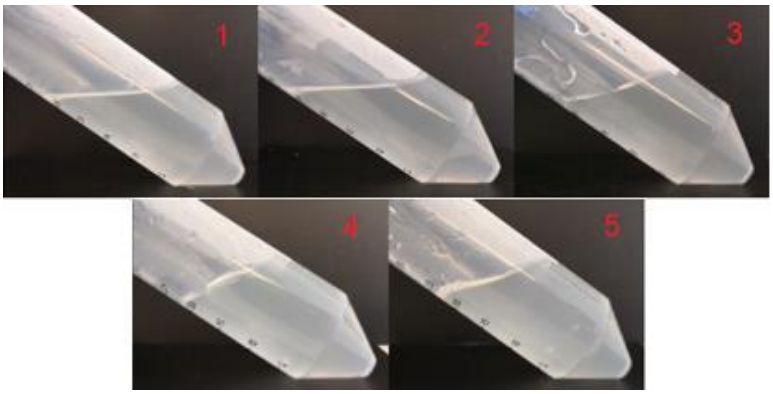

Figure 17 Binder Solution #4 (kCar_2.7wt%_80°C): (1) Hot Status; (2) T_{room}; (3) Day 2; (4) Day 3; (5) Day 7

Things became interesting when investigating the gel behavior of new purchased kCar powder from Melbourne Food Depot after running out of original kCar powder. When 1 wt% concentrated solutions were fabricated with old and new kCar powder, they displayed completely different gel behavior after cooling down as shown in Figure 18.

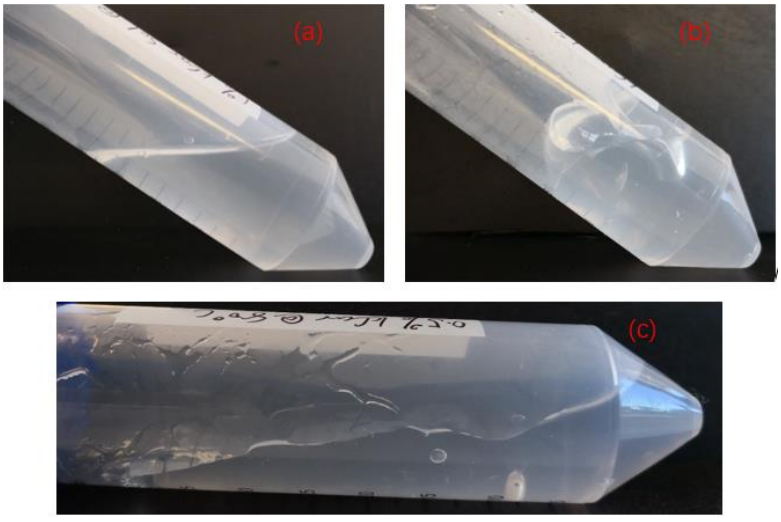

Figure 18 (a) solution #6 (kCar_1wt%_80°C) (b) solution #7 (new kCar_1wt%_80°C) (c) solution #8 (new kCar_0.5wt%_80°C)

The solution #6 (kCar_1wt%_80°C) in Figure 18 (a) did not form any gel structures but smoothly-flowing liquid. The solution #7 (new kCar_1wt%_80°C), however, developed into a gel that was too brittle to exhibit any flowing behavior and integrate into solid bulk. This gel structure was even thicker than the gel formed in a solution of 2.7 wt% old kCar powder shown in Figure 17. Meanwhile, solution #8 (new kCar_0.5wt%_80°C) was also produced shown in Figure 18 (c). This solution also exhibited soft gel with weak cross-linked system. There were definitely different components in kCar powders from different sources and detailed SEM and EDS analysis were conducted and presented in section **Error! Reference source not found.**.

4.1.2 Potential Influence Factors of Adhesion

The attachment between the cathode layer and the current collector would significantly influence the electrochemical performance of batteries. Poor adhesion of binder might generate cracks on the cathode surface and even causes separation of cathode layer from the current collector. This section will then investigation factors possibly influencing the adhesive strength of carrageenan powder.

4.1.2.1 Different Temperature of Binder Solution

Solution #1 (iCar_0.2wt%_80°C) was used to produce two 1.75 wt% iCar cathodes. All procedures and composition were identical to these cathodes except the temperature of iCar solution during mixing, where one adopted 80 °C solution and the other used solution of room temperature. Figure 19 shows the adhesion status of these two cathodes after punch.

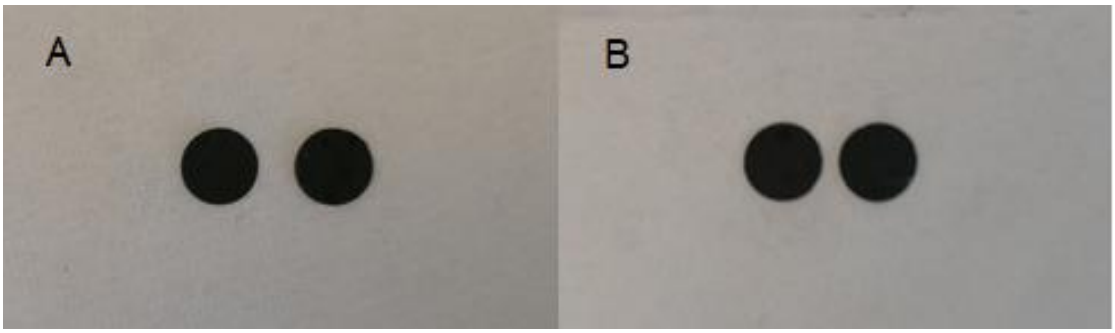

Figure 19 (A) Cathode with iCar solution of 80 °C (B) Cathode with iCar solution of T_{room}

Although the temperature of the iCar solution used for slurry mixing was different, final samples both presented strong adhesion between the cathode and current collector. Therefore, the effect of temperature during mixing on adhesive strength was negligible, while the effect on the dispersion of active material and cycling performance needed to be determined within further experiments.

4.1.2.2 Different Heating Temperature of Binder Solution

Another potential factor influencing the adhesive strength might be the heating temperature

during the production of binder solution since the carrageenan powder would only be soluble in water at a temperature higher than 60 °C. With other conditions fixed, binder solution #1 (iCar_0.2wt%_80°C) and #5 (iCar_0.2wt%_40°C) were only different in heating temperature and two cathodes were fabricated using these two binders respectively. The comparison of adhesion strength for two cathodes is shown in Figure 20.

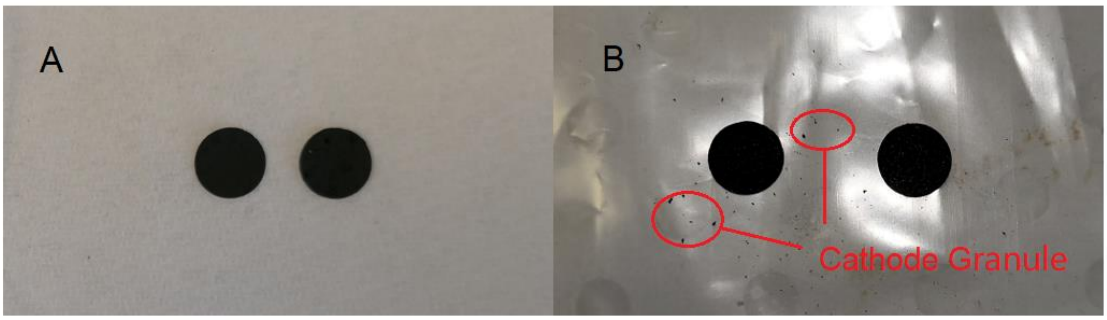

Figure 20 (A) Cathode with solution #1 (iCar_0.2wt%_80°C) (B) Cathode with solution #5 (iCar_0.2wt%_60°C)

The cathode fabricated with solution #5 (iCar_0.2wt%_40°C) exhibited good attachment to the current collector but with the appearance of a little cathode granule, which was peeled off during punching. This phenomenon demonstrated the inferior adhesive strength of cathode created with solution #5 (iCar_0.2wt%_40°C) compared to the previous one. The binder solution seemed not to dissolve in water completely at 60 °C with large agglomerates surrounded by film layer shown in Figure 21. These cathodes were still feasible to construct into batteries but an investigation about the electrochemical performance was required.

Figure 21 Solution #5 (iCar_0.2wt%_40°C) with agglomerates in red circle

4.1.2.3 Different Viscosity between iCar and kCar

Due to the distinctive fluidity behavior of the binder solution of iCar and kCar observed in section 4.1.1, the adhesive strength between the cathode and current collector might also be different for those two binders with same concentration. Hence, two cathodes were fabricated

with binder solution #1 (iCar_0.2wt%_80°C) and #3 (kCar_0.2wt%_80°C) to examine whether iCar and kCar would present different adhesion performance. The result of two cathodes is shown in Figure 22.

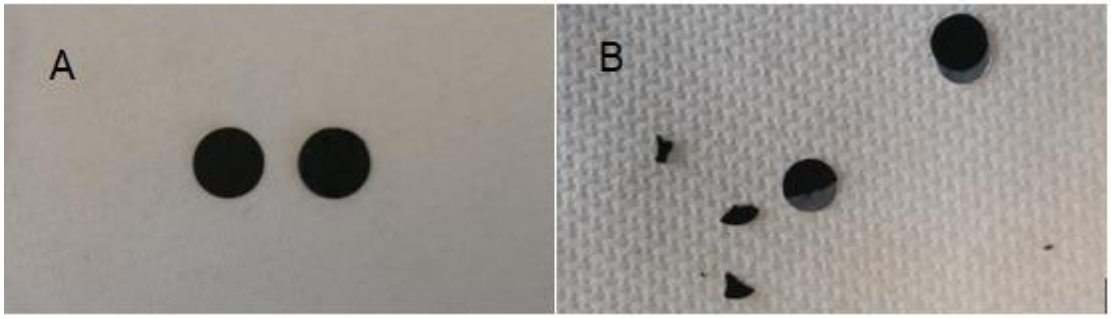

Figure 22 (A) Cathode with binder solution #1 (iCar_0.2wt%_80°C) (B) Cathode with binder solution #3 (kCar_0.2wt%_80°C)

While cathode composed of iCar binder remained intact after punching into coin shape, cathode with the same amount of kCar binder manifests weak adhesion, resulting in crumbled and delaminated cathode layer. 1.75 wt% of kCar binder was not enough to produce qualified cathode and a sufficient proportion of kCar binder in cathode needed to be determined.

Meanwhile, the efforts to produce cathode with binder solution #7 (new kCar_1wt%_80°C) failed since the pipette could not even extract small quantities of solution from its brittle gel structure. Hence, cathode with 5 wt% of kappa carrageenan binder was then produced using solution #8 (new kCar_0.5wt%_80°C) and presented in Figure 23.

Figure 23 5 wt% kCar Cathode with solution #8 (new kCar_0.5wt%_80°C) and aggregated portions circled in red

The cathode presented certainly inhomogeneous dispersion of active material and could be classified into two types of regions. The darker regions circled with red lines were aggregated active material including sulfur and carbon elements without any binder components. Therefore, those areas were fragile and less adhesive to the current collector. Other regions of cathode exhibited less content of sulfur element and minor cracks, which caused overestimation of sulfur loading. The cathodes fabricated by new kCar, thus, were inappropriate to assemble into

batteries for comparison due to their uncertainties of structural integrity and sulfur loading.

4.2 The Thickness and Sulfur Loading of Cathodes

While cathodes were produced according to compositions listed in Table 3 and punched into disks of 8 mm diameter, the weight of cathode disks would then be weighted on a scale. The slurry layer coated on the current collector was not uniform. As such, the sulfur loading of the dried cathode would vary according to its position. Generally, the cathodes punched at the middle of deposition tended to exhibit a thicker layer and higher sulfur loading whereas the cathodes punched at the side of deposition would have lower sulfur loading. This phenomenon may be caused by the high fluidity of slurry mixture produced with addition of a large amount of solution.

This measurement would detriment the surface of the cathode. Except for those with sulfur loading around 2.5 g/cm2, all cathodes would go through thickness measurement with micrometer screw gauge in order to find the correlation between sulfur loading and thickness. All raw data have been fitted into two categories based on their composition and presented in appendix A with equations of calculating sulfur loading. A diagrammatic demonstration with thickness against sulfur loading is shown in Figure 24.

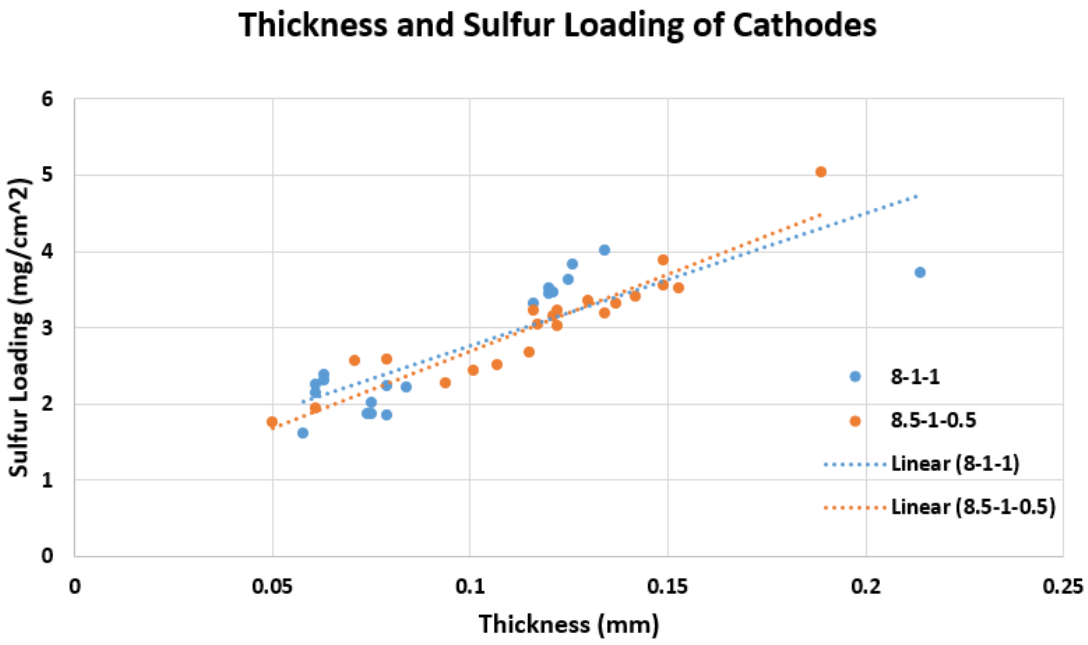

Figure 24 Relationship between Thickness and Sulfur Loading of Cathodes based on different compositions

Cathodes with different compositions both showed evident linear correlation between thickness and sulfur loading, where thicker cathodes generally possess higher sulfur loading. Some outliers, however, were also observed from the diagram for cathodes with comparatively larger

thickness. They showed either higher sulfur loading than the trendline predicted or lower.

4.3 EDS Analysis of Carrageenan Powder

Since the kappa and iota carrageenan powders were received from two different sources named in section 3.1.1 and new kCar powder displayed different gel behavior in section 4.1.1, the comparison between compositions of powder was conducted under energy-dispersive X-ray spectroscopy. The analyses of old powders were conducted by equipment SU3500 and TM3030 were adopted for new powders.

4.3.1 Iota Carrageenan

The iCar powder from different sources was investigated at first. The EDS analysis of old iCar powder bought from Sigma-Aldrich was shown in Figure 25 and counterpart of new iCar powder from Melbourne Food Depot was shown in Figure 26.

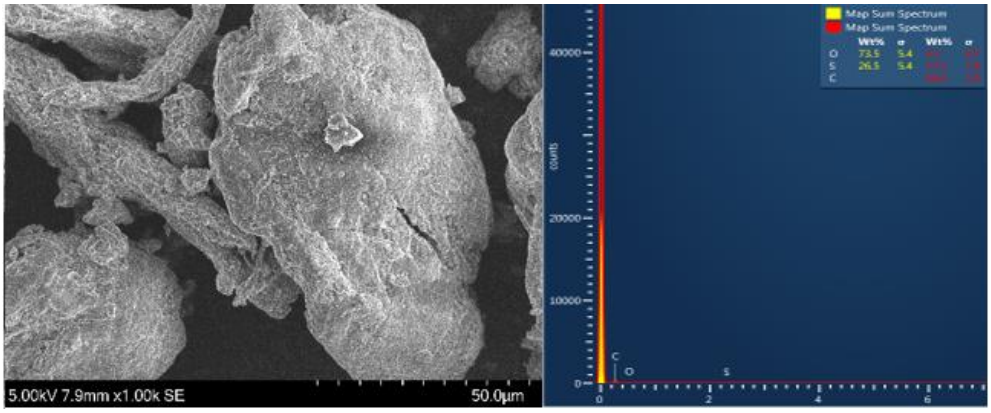

Figure 25 (a) SEM Image of Old iCar under 1k Times Magnification (b) EDS Analysis Spectrum

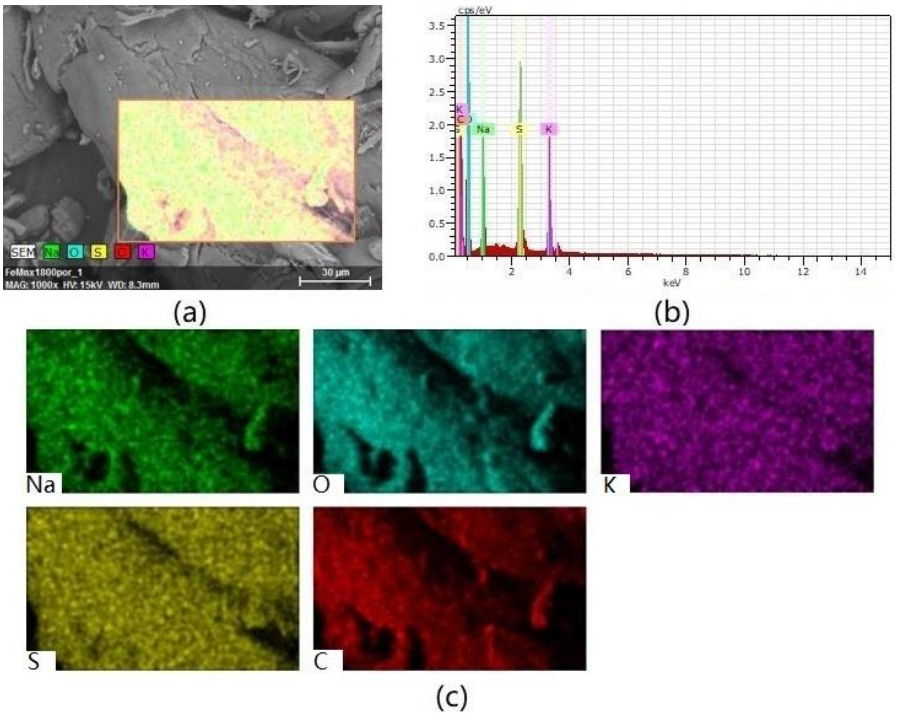

Figure 26 (a) SEM Image of New iCar under 1k Times Magnification (b) EDS Analysis Spectrum (c) Elements

In Figure 25, the old iCar showed chemical elements of carbon, oxygen and sulfur without the presence of any other contaminations. However, the EDS analysis spectrum of new iCar powder showed the existence of other elements including sodium (shown as green) and potassium (shown as purple). From the elemental mappings shown in Figure 26 (c), the distribution of sodium shared the same area as oxygen and carbon, while potassium element coincided with sulfur particle. These overlapping indicated that those impurities were bonded with ester sulfate groups and carbon atoms in new iCar powder.

4.3.2 Kappa Carrageenan

The two different kCar powders were also investigated. The EDS analysis of old kCar powder bought from Sigma-Aldrich would be present first in Figure 27 and the same analysis of new kCar powder is shown in Figure 28.

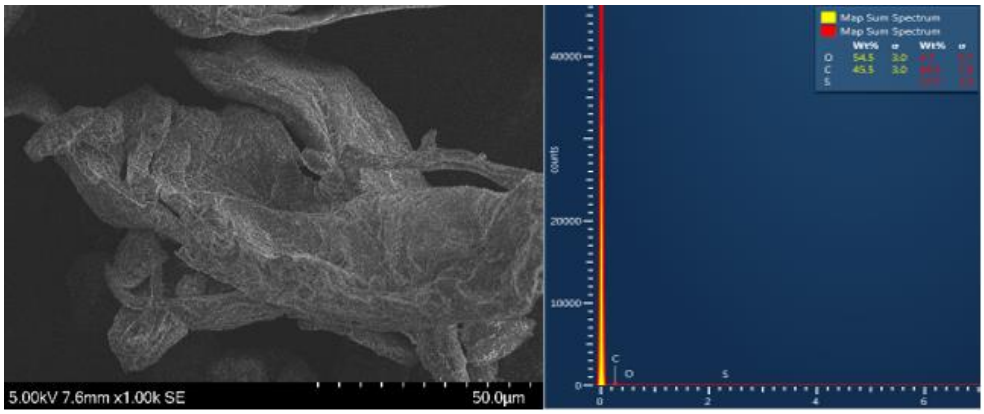

Figure 27 (a) SEM Image of Old kCar under 1k Times Magnification (b) EDS Analysis Spectrum

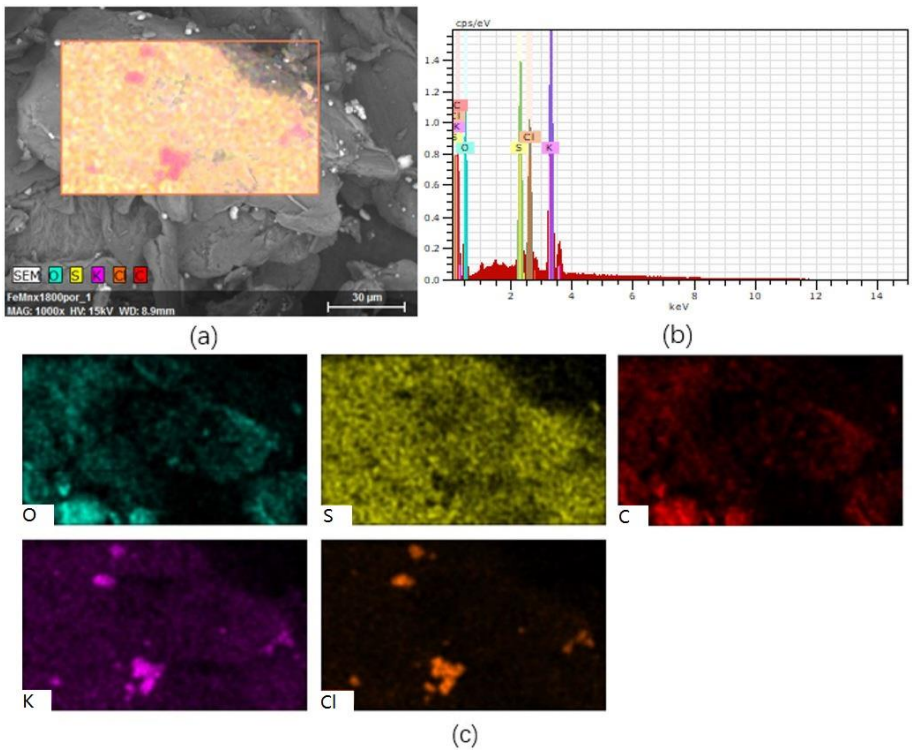

Figure 28 (a) SEM Image of New kCar under 1k Times Magnification (b) EDS Analysis Spectrum (c) Elements Distribution in Selected Area

The EDS analysis of old kCar in Figure 27 shows that old kCar powder was not contaminated by other elements, with all expected ingredients. The new kCar powder, nevertheless, showed exotic elements of potassium (purple) and chlorine (orange). Unlike the new iCar powder, in which contaminations were boned with carrageenan, new kCar powder showed the presence of contaminated bulks as shown in Figure 28 (a) and Figure 28 (c) also presented the overlapping distribution of potassium and chlorine. The pollutant was considered to be compound KCl, which would facilitate the formation of gel in kCar solution referring to Section 2.1.5.2.

4.4 SEM Analysis of Cathodes

Figure 29 shows the SEM figures of cathodes composed of 5 wt% and 10 wt% PVDF and iCar binders under lower magnification. All cathodes showed different sizes of cracks and void space, which were the dark lines and spots spread over the cathode surface. The defects of PVDF-based cathode were more obvious and frequently appeared than counterparts of iCar-based one. Meanwhile, the large bright flakes on PVDF-based cathodes were sulfur particles as confirmed by EDS analysis. The existence of bulk sulfur element implicated insufficient dispersion of active material in PVDF-based cathode, which might detriments the electrochemical performance of cells made from that cathode. The sulfur in iCar-based cathodes showed a uniform distribution of active material without any large flakes of sulfur bulk. Small defects were also observed in Figure 29 (c) and (d) but were negligible to the whole.

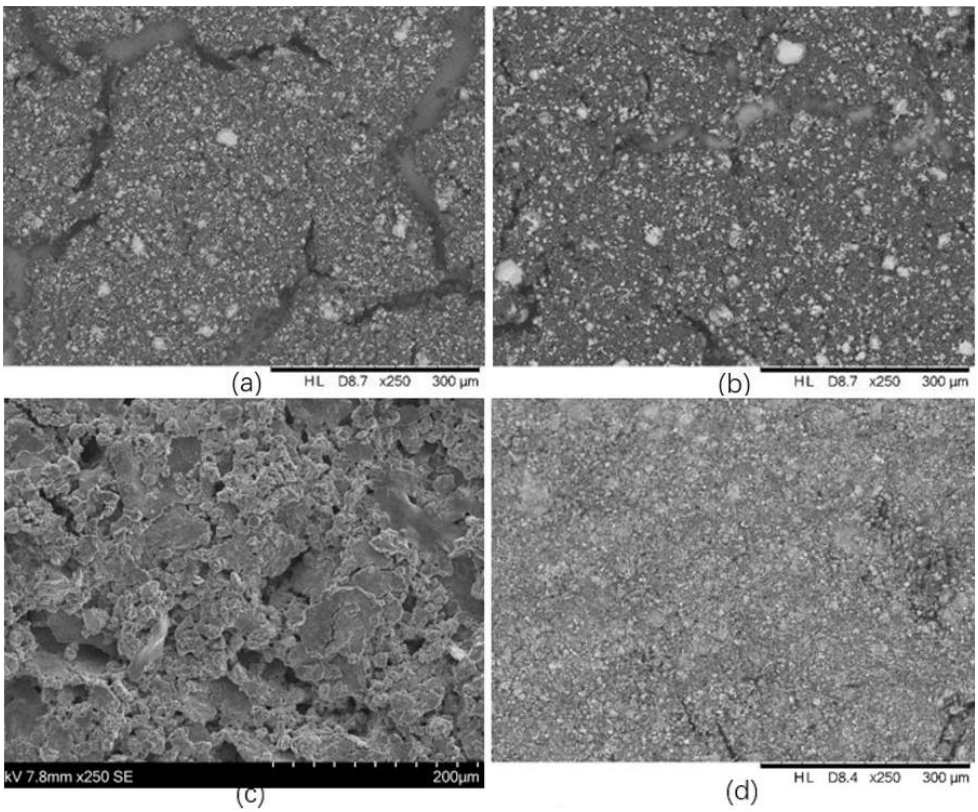

Figure 29 SEM at Lower Magnification (a) PVDF-5% (b) PVDF-10% (c) iCar-5% (d) iCar-10%

In the SEM figures with higher magnification shown in Figure 30, the difference of sulfur element dispersion on surface of iCar and PVDF based cathodes was more distinctive, where a large number of bulk sulfur particles existed in the PVDF-based cathodes. At the same time, the proportion of bright area in Figure 30 (a) was relatively higher than that of 10 wt% one, which corresponds to the higher composition of active material and sulfur loading within 5 wt% PVDF cathode. A large bulk of sulfur was also observed in the middle of Figure 30 (b). In general, PVDF binder did not coat on the active materials in the cathode, but only stick all different types of content together.

On the other hand, cathodes with iCar binder presented lighter figures since sulfur particles were dispersed on the surface more homogeneously. Figure 30 (c) was shot by SU3500 (higher resolution machine) with details of different-depth layers. Figure 30 (d) was slightly blurred due to the mottled effect generating by the gel structure of iCar binder.

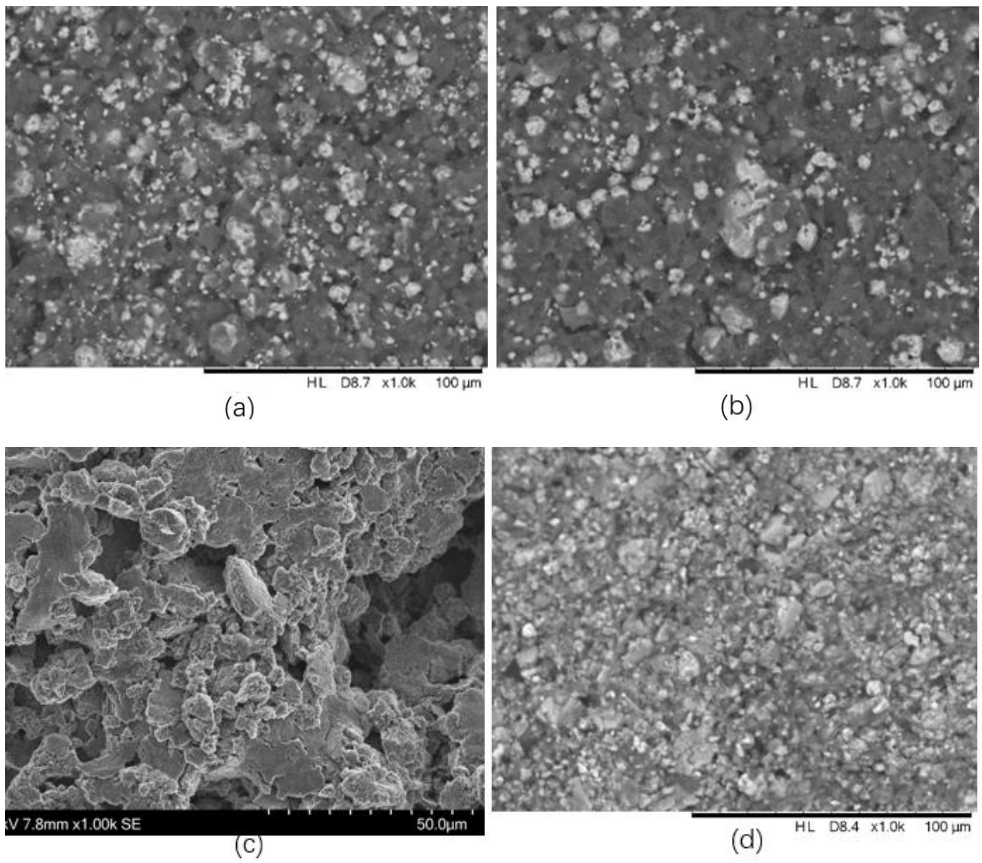

Figure 30 SEM at Higher Magnification (a) PVDF-5% (b) PVDF-10% (c) iCar-5% (d) iCar-10%

4.5 EDS Analysis of Cathodes

This section presents the analyses of elements distribution for different cathodes under EDS analysis.

4.5.1 PVDF Based Cathodes

The EDS analyses of PVDF-based cathodes with 5 wt% and 10 wt% binder were conducted and presented in Figure 31 and Figure 32. The EDS method primarily investigated the elemental content and distribution of cathode.

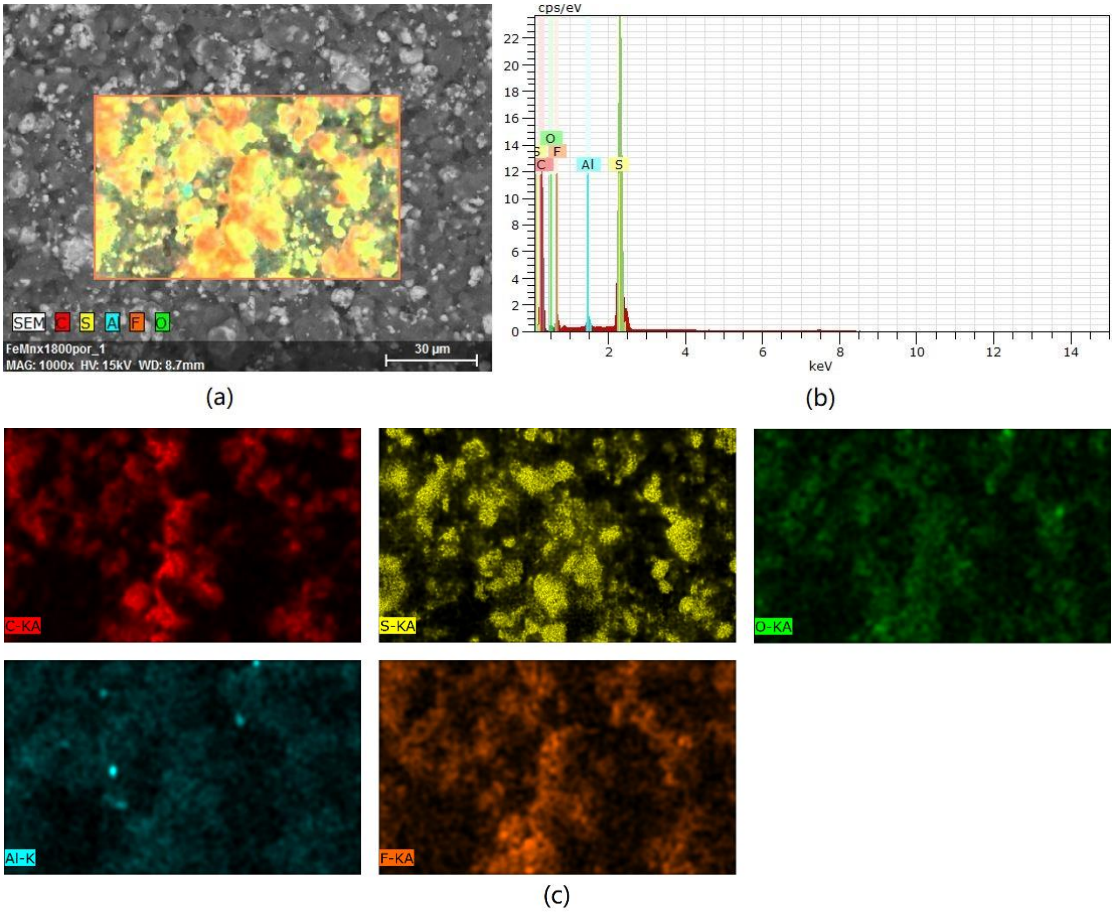

Figure 31 (a) SEM Image of Cathode with 5 wt% PVDF under 1k Times Magnification (b) EDS Analysis Spectrum (c) Elements Distribution in the Selected Area

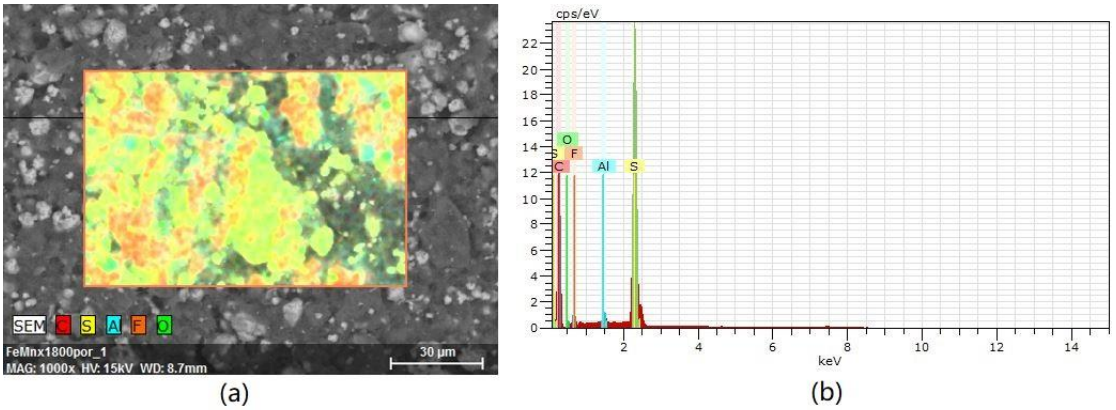

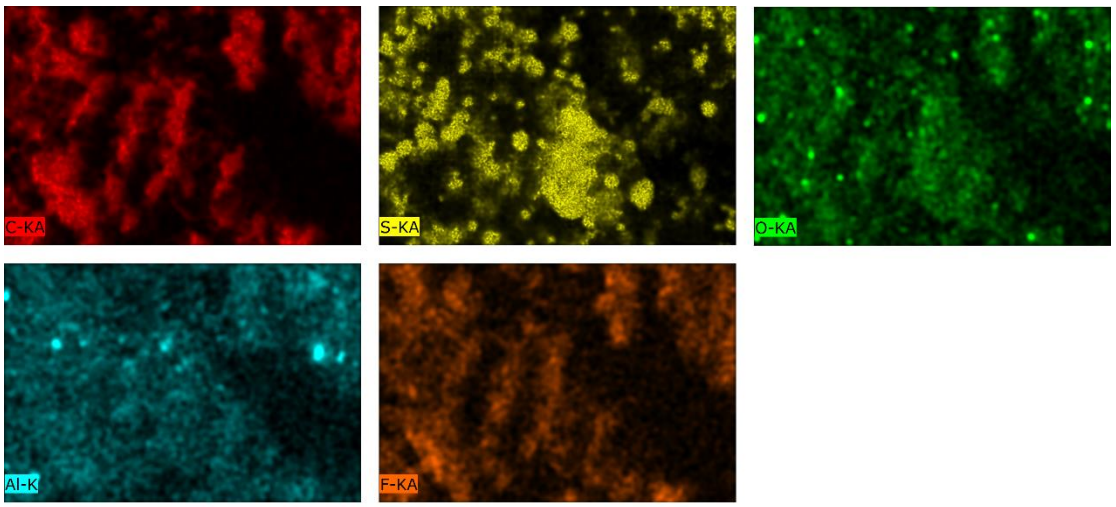

(c)

Figure 32 (a) SEM Image of Cathode with 10 wt% PVDF under 1k Times Magnification (b) EDS Analysis Spectrum (c) Elements Distribution in the Selected Area

The composition of elements in both PVDF-based cathodes consisted of oxygen, carbon, sulfur, fluorine, and aluminum, which were consistent with all expected elemental components without the existence of any contaminations. Fluorine and carbon were from PVDF binder and electronic conductor respectively. The appearance of aluminum element may be sourced from the current collector. The distribution of carbon (red) and fluorine (orange) overlapped with each other for both cathodes, yet sulfur was separated from carbon. At the same time, the sulfur element dominated the configuration of both cathodes regarding the EDS spectrum given and the cathode with 85 wt% of active material possessed more sulfur particles with the yellow color in the EDS images.

4.5.2 iCar Based Cathodes

Figure 33 and Figure 34 below provide the EDS results of iCar-based cathodes with 5 wt% and 10 wt% binder. The EDS analysis for 5 wt% one, performed by SU3500, only consisted of SEM image and elemental spectrum without the distribution map.

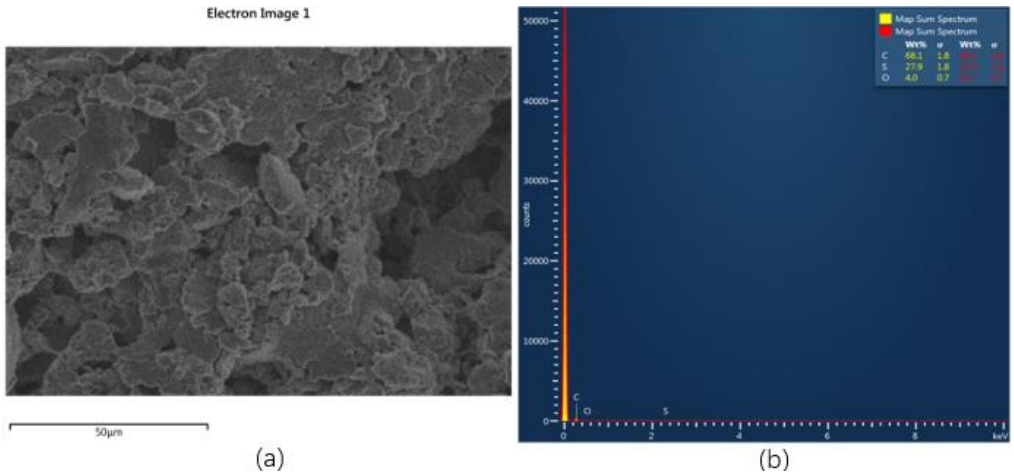

(a) (b)

Figure 33 (a) SEM Image of Cathode with 5 wt% iCar under 1k Times Magnification (b) EDS Analysis Spectrum

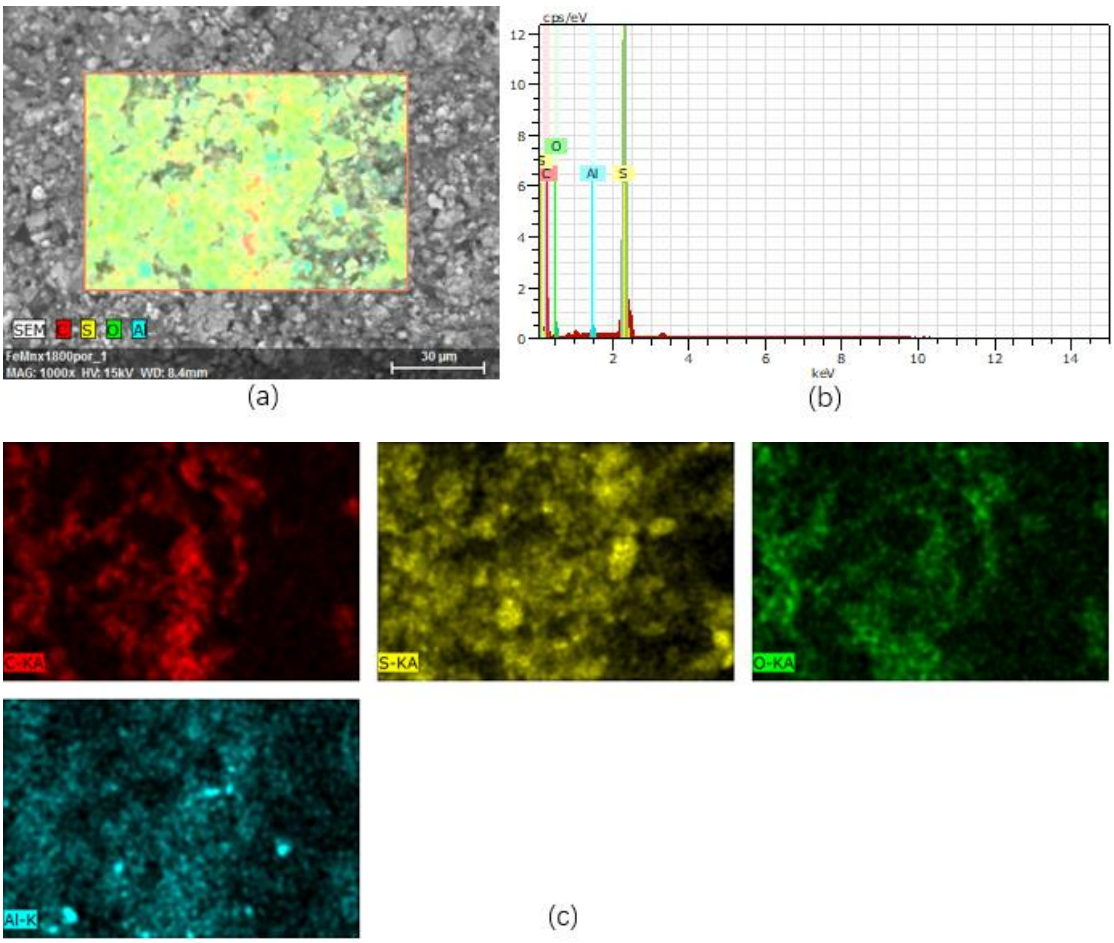

Figure 34 (a) SEM Image of Cathode with 10 wt% iCar under 1k Times Magnification (b) EDS Analysis Spectrum (c) Elements Distribution in the Selected Area

From Figure 33 and Figure 34, it could be observed that carbon, oxygen and sulfur elements existed in both iCar cathodes, but there was the trace of aluminum element only in 10 wt% iCar cathode, while the 5 wt% cathode did not have any contamination. Meanwhile, up to 68.1 wt%, carbon element dominated the inspected surface area of 5 wt% cathode while the sulfur element occupied the most surface area in 10 wt% cathode as shown in Figure 34 (b).

4.6 Testing of Preliminary Battery with iCar

This section presents the battery testing results of initially constructed cells. The cathodes used in these batteries were bound by iota carrageenan and dried in a vacuum oven at 60 °C overnight. The sulfur loading of battery with 5 wt% and 10 wt% iCar was 2.62 mg/cm2 and 2.53 mg/cm2 respectively.

4.6.1 OCV Testing

The OCV testing measured the electrochemical potential between two electrodes of cells. A freshly fabricated or fully charged LSB should display a voltage around 2.2-2.3 V if the battery is functional. A short-circuited battery would present a voltage around 0 in OCV testing. Figure 35 shows an OCV testing of iCar based cathodes with 5 wt% and 10 wt% binder, where the

dashed and solid lines represent the OCV before and after cycling test respectively. All OCV lines have minor fluctuations over time and mainly fix on a constant voltage. The battery with the higher iCar exhibited a larger OCV and voltage potential increases after cycling test for both batteries, which implies an increment on the electromotive force.

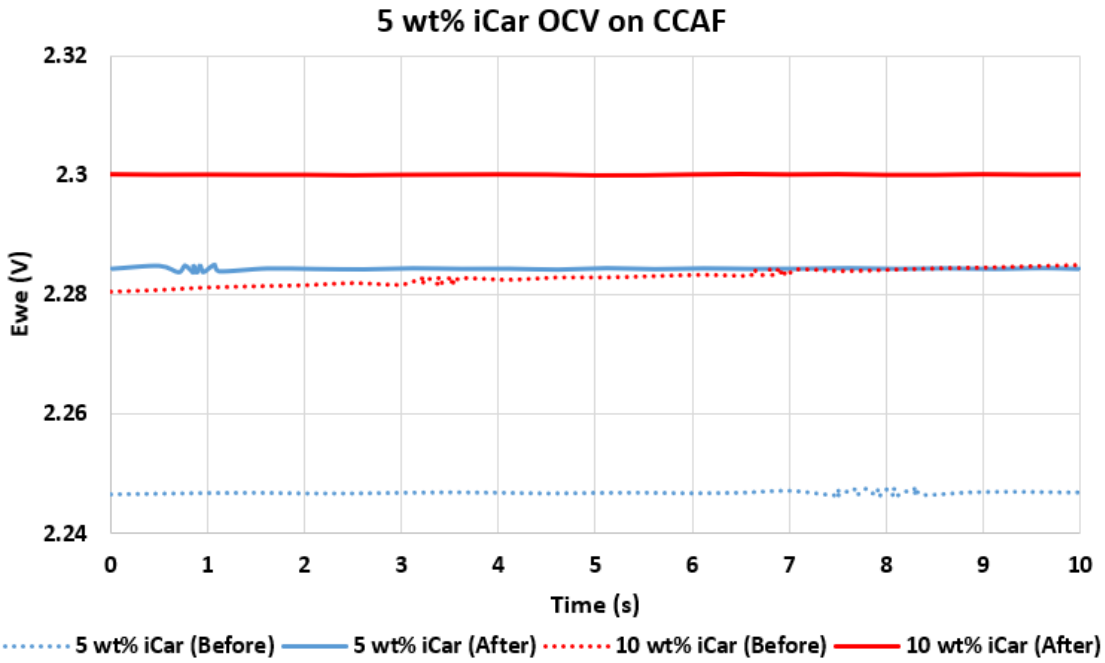

Figure 35 OCV Comparison between Batteries with Different Binder Proportion

4.6.2 EIS Testing

The results of EIS were presented in the Nyquist plot shown as Figure 36 for battery with 5 wt% iCar binder and Figure 37 for the cell with 10 wt%. Since the maximum testing frequency was only 100 kHz initially, it was not high enough to show the intersection between impedance response curve and the axis of real impedance referred to Figure 12. Therefore, black semicircles at high-frequency range were fit into the impedance response to predict the ohmic resistance of cells. The diameter of black semicircles also indicated charge transfer impedance of polysulfide intermediates [71] (refer to the modeling of LSB in EIS chart in section 3.3.2).

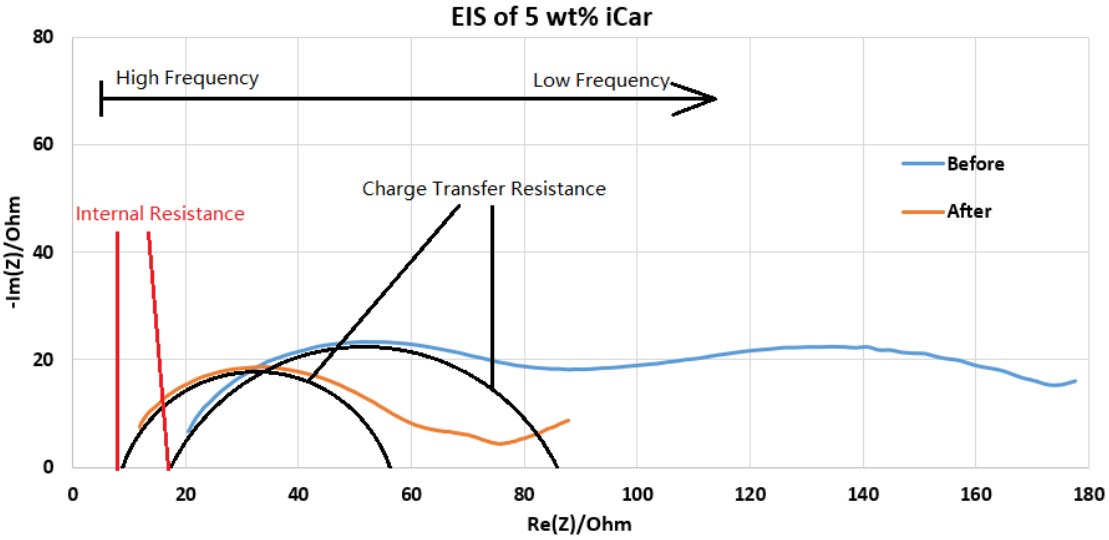

Figure 36 EIS Analysis of Preliminary Battery with 5 wt% iCar

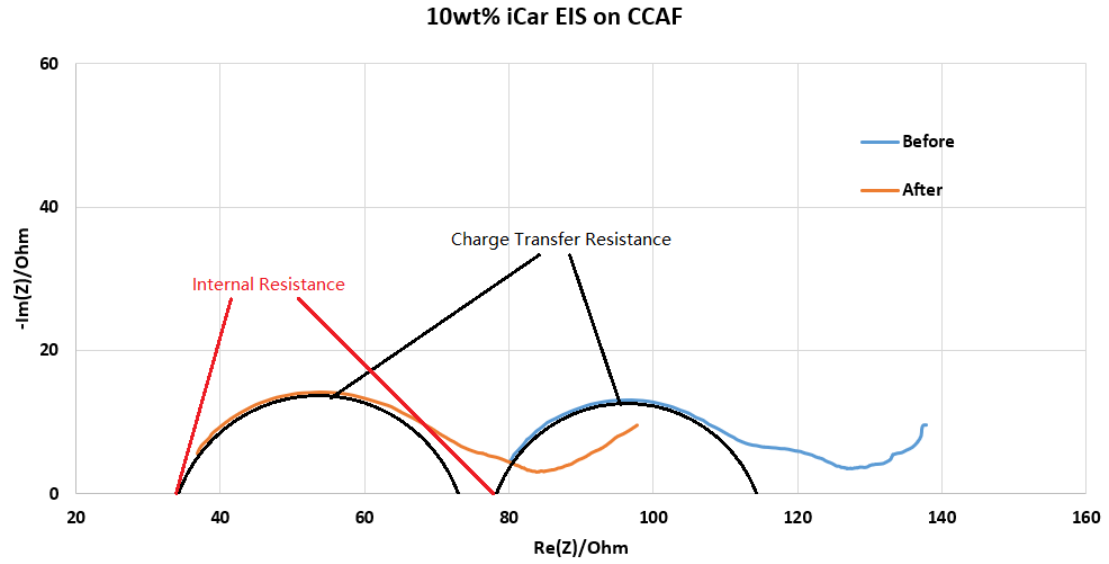

Figure 37 EIS Analysis of Preliminary Battery with 10 wt% iCar

The battery with 10 wt% of iCar binder could be seen to have the highest ohmic resistance (R_S) around 78 ohms before cycling, but it dropped significantly down to 33 ohms after testing. Another cell also demonstrated reduction of R_S from 18 to 9 ohms after the cycling test. The battery with 5 wt% of iCar before cycling showed the largest charge transfer resistance (R_{CT}) around 67 ohms, while the other only exhibited 35 ohms impedance within the polysulfide intermediates. The R_{CT}, however, showed different changing patterns, which was decreased in 5 wt% iCar battery after cycling test but slightly increased in 10 wt% iCar battery.

4.6.3 Cycling Testing

Cycling testing results of both batteries were presented in this section. Figure 38 showed the voltage profiles of 5 wt% and 10 wt% iCar batteries against specific discharging capacity at different cycles.

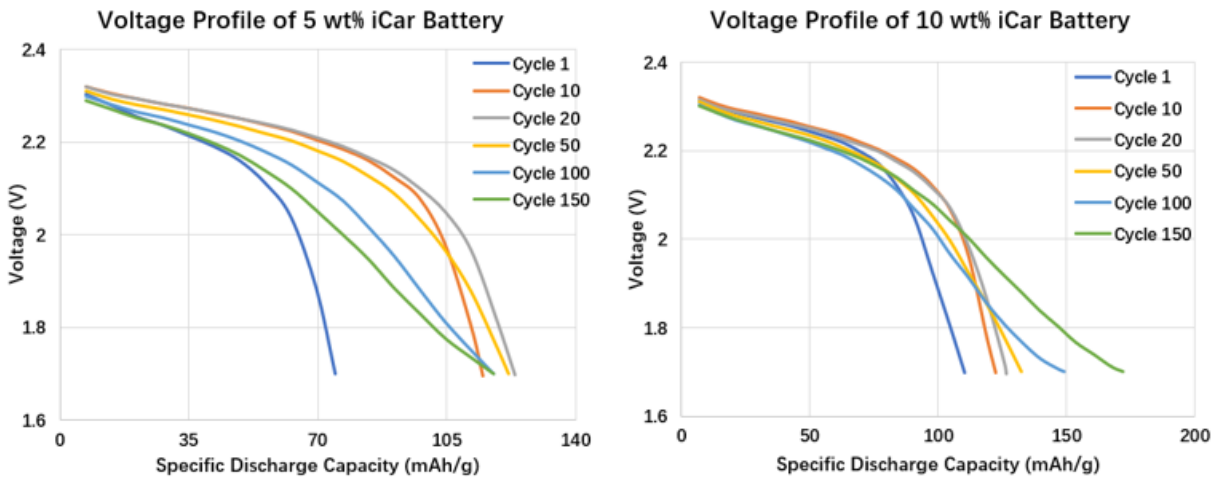

Figure 38 Voltage Profile against Specific Discharge Capacity

The normal LSB should present two constant voltage plateaus around 2.2 V and 2 V as shown in Section 2.2, coinciding to the reduction from elemental sulfur to Li_2S_8 and from Li_2S_8 to Li_2S_6 and Li_2S_4 respectively. After experiencing the first voltage plateau, however, the voltage of both preliminary cells dropped rapidly to cut-off value without any exhibition of second voltage plateau at all. Since assembly of batteries was operated in the glovebox, this phenomenon implicated that impurities were introduced to the cathode during fabrication and participated in electrochemical reaction with sulfur. No extra element was detected by EDS analyses; hence, the impurities were initially judged as residual moisture from the binder solution.

Meanwhile, suddenly falling of voltage also did not contribute discharging energy and resulted in impairment on specific discharging capacity, which is only around 5% of theoretical energy density. Without showing a declining trend, the discharging capacity of both preliminary batteries was increasing along with cycling number. This abnormal situation also indicated insufficient utilization of active material in batteries.

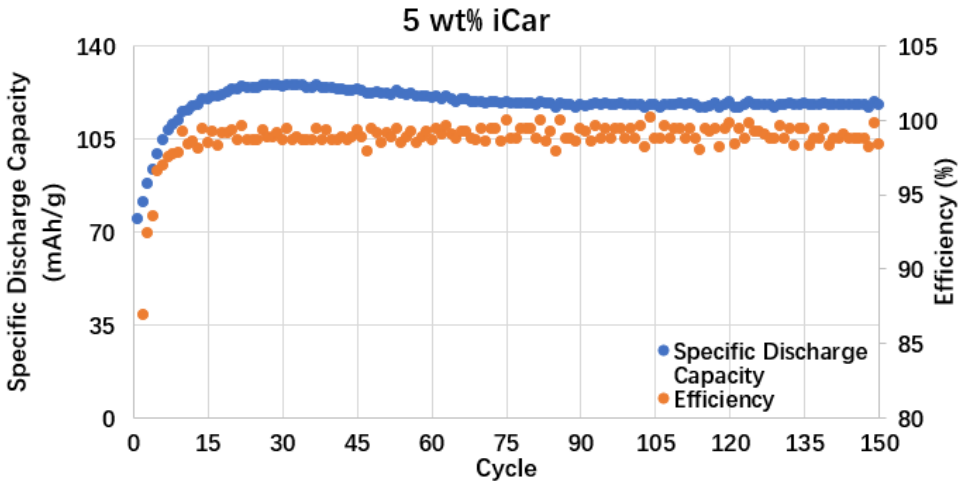

Figure 39 Specific Discharging Capacity and Efficiency against Cycles for 5 wt% iCar Cell

The specimen with 5 wt% iCar binder only possessed a specific capacity of 74.5 mAh/g and 43.3% efficiency in the first cycle as shown in Figure 39. The efficiency then rapidly improved to 98% and fluctuated around this value for later cycles. The specific discharging capacity also increased after initial cycles to the peak of 125.2 mAh/g and then glissaded gradually to 98.1 mAh/g at the end of the cycling test.

Figure 40 below presented the cycling result of battery with 10 wt% iCar. It displayed higher initial specific discharging capacity and efficiency compared to those of previous one. The efficiency also fluctuated around 98% and even exceeded 100% sometimes. Unlike the slightly declining trend shown in the former figure, this cell maintained its growing pattern until the end of the cycling test and reached 180.1 mAh/g.

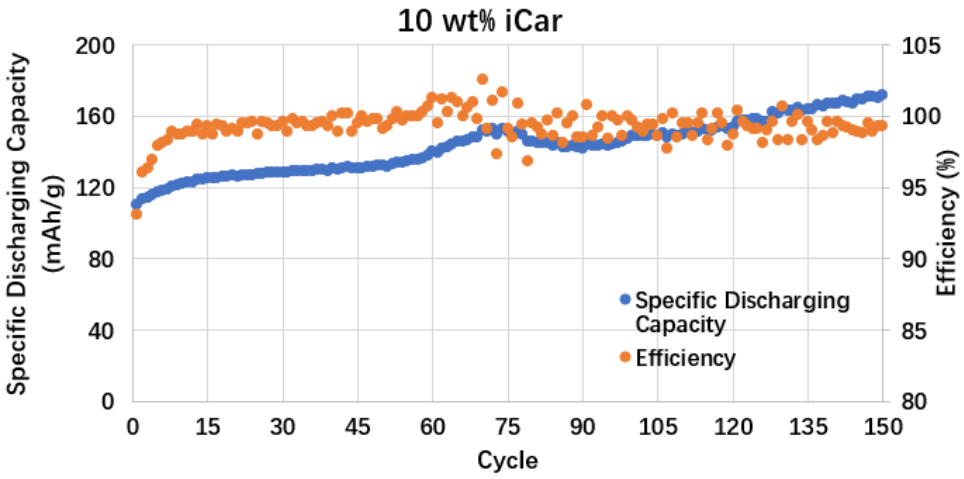

Figure 40 Specific Discharging Capacity and Efficiency against Cycles for 10 wt% iCar Cell

4.7 Testing of Final Battery with PVDF and iCar

After increasing the temperature of drying cathode from 60 °C to 70 °C in the vacuum oven, the problem existed in preliminary batteries has been fixed. Two iCar based batteries of 8:1:1 and 8.5:1:0.5 (CNT60: SP: binder) compositions were fabricated again with sulfur loading of 2.577 mg/cm^2 and 2.569 mg/cm^2 respectively. With sulfur loading of 2.093 mg/cm^2 and 2.384 mg/cm^2, two PVDF-based cells of same compositions were also constructed for comparison. The battery testing results are illustrated in this section with a focus on the comparison between batteries of same content ratio.

4.7.1 OCV Testing

The OCV testing results of four types of batteries were presented in Figure 41. Each type of battery showed an OCV before and after cycling test represented by dashed and solid lines respectively. Unlike the OCV results of preliminary batteries, all valid cells displayed a reduction of electromotive force to some extent. Battery with 10 wt% PVDF showed a

substantial decline of 0.23 V after cycling test, while others dropped around 0.19 V. Meanwhile, fluctuation of OCV could also be observed for these cells.

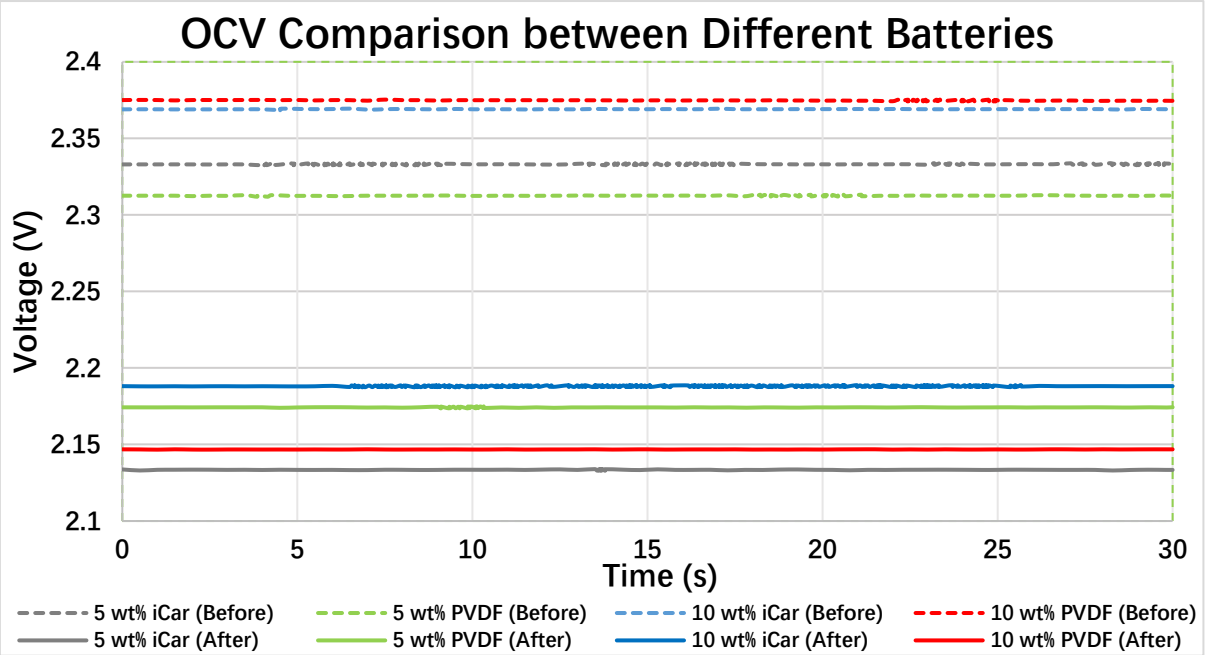

Figure 41 OCV Comparison between Different Batteries

4.7.2 EIS Testing

Figure 42 presents the EIS results of iCar and PVDF based batteries with 5 wt% and 10 wt% binder content. All internal resistances (R_S) and charge transfer resistances (R_{CT}) of four cells were determined from those figures and recorded in Table 5. Cells with 5 wt% binder showed higher R_S but lower R_{CT} initially. R_S decreased after cycling test while R_{CT} increased. Cells with 10 wt% binder, however, displayed opposite behaviors, where R_S increased but R_{CT} declined after cycling test. Under the same composition, iCar based batteries exhibited lower R_S throughout and higher R_{CT} at the end.

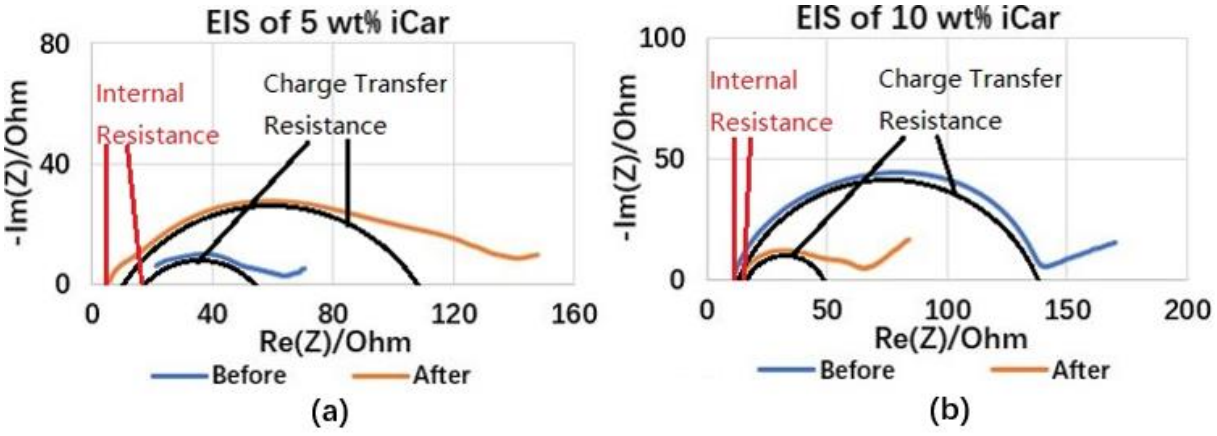

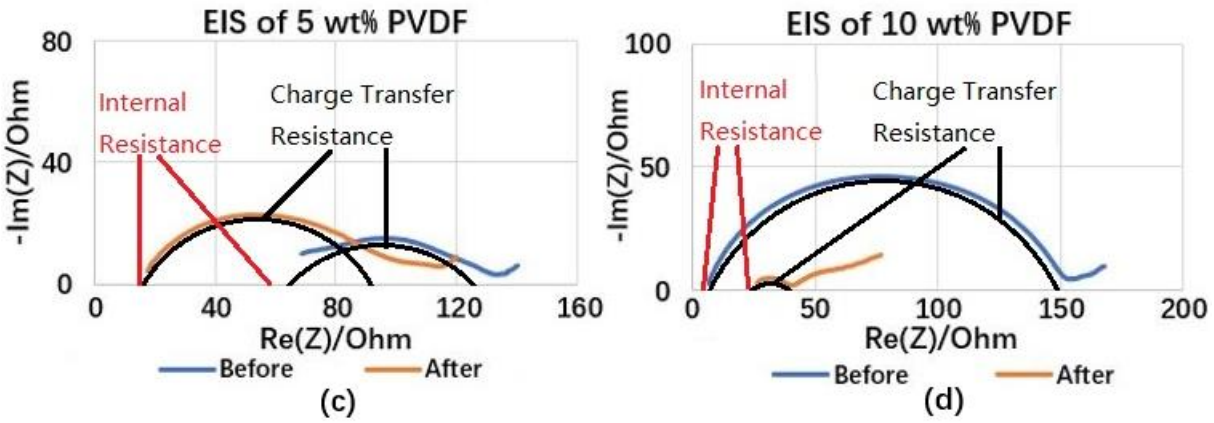

Figure 42 EIS Testing of Batteries with (a) 5 wt% iCar (b) 10 wt% iCar (c) 5 wt% PVDF (d) 10 wt% PVDF

Table 5 Internal Resistance & Charge Transfer Resistance of Four Types of Battery

Battery Type	R_S Before (Ohms)	R_S After (Ohms)	R_{CT} Before (Ohms)	R_{CT} After (Ohms)
5 wt% iCar	17	6.1	38.4	96
10 wt% iCar	11	15	124	32
5 wt% PVDF	58	17	60.8	73.6
10 wt% PVDF	6.5	23	140	20

4.7.3 Cycling Testing

The cycling results of four different batteries were shown in Figure 43, Figure 44 and Figure 45. In Figure 43, all batteries presented voltage plateau around 2 V except the first cycle of the cell with 5 wt% PVDF binder. The initial voltage potential of 5 wt% PVDF cell dropped to 1.75 V but raised back to 2 V later. The voltage profile of 10 wt% iCar battery was unstable, dropping from 2V to 1.9 V with a slight gradient. At the same time, the specific capacity of all cells showed a decreasing trend after the first cycle.

Figure 44 compared specific discharging capacity of different cells. Battery with less content of binder generated higher specific capacity initially but showed less capacity retention after the test. The battery of 5 wt% PVDF, which owned the highest initial specific capacity of 623.4 mAh/g, decayed dramatically to 330 mAh/g after 150 cycles. 10 wt% PVDF battery also showed rapid degradation of capacity during cycling test from 481.2 mAh/g to 271.6 mAh/g. Cells with PVDF binder both demonstrated more than 40 % capacity decaying rate after 150 cycles. In contrast, cells with iCar binder exhibited better capacity retention rate, which maintained 63% and 77% of initial discharging capacity for 5 wt% and 10 wt% iCar binder respectively. Their maximum specific discharging capacities were 511 mAh/g and 457 mAh/g. The cell with more iCar binder proved to possess the best cyclability performance.

At last, the coulombic efficiency of different cells was compared in Figure 45 across 150 cycles. Battery with 5 wt% iCar showed the highest and the most stable efficiency around 99% among

all cells. Cell composed of 10 wt% iCar, however, exhibited lowest average efficiency around 95% but still stable. The efficiency of PVDF based batteries both experienced a reduction of 2% after 150 cycling tests.

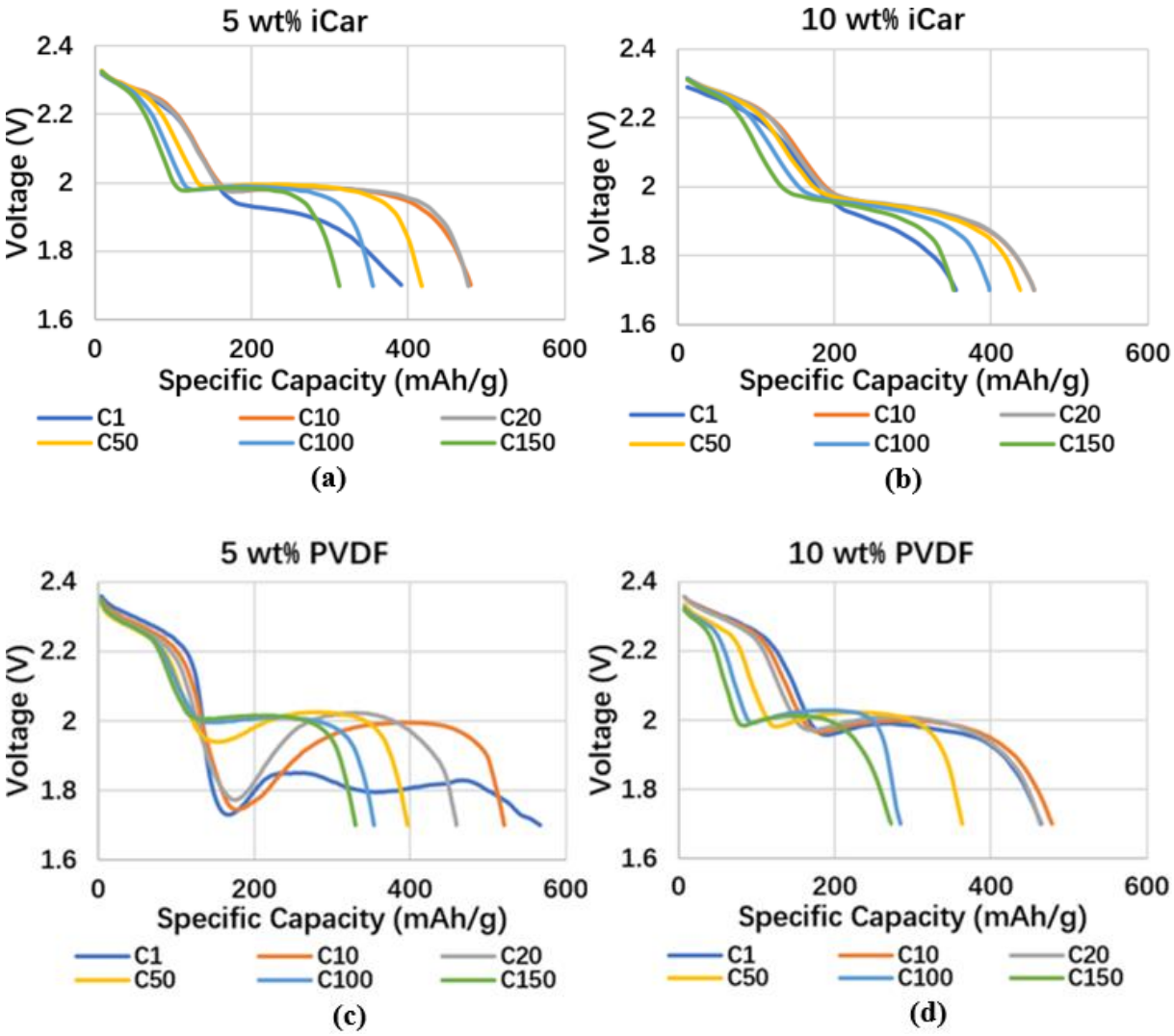

Figure 43 Voltage Profile of Batteries with (a) 5 wt% iCar (b) 10 wt% iCar (c) 5 wt% PVDF (d) 10 wt% PVDF

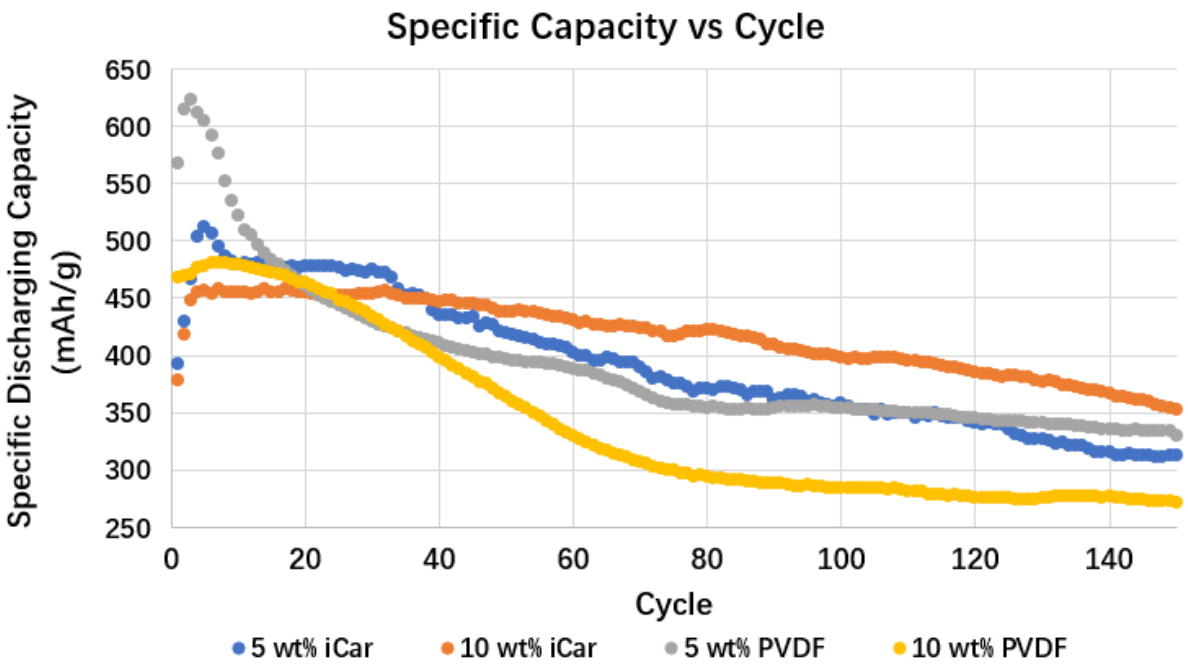

Figure 44 Specific Discharging Capacity of Different Cells

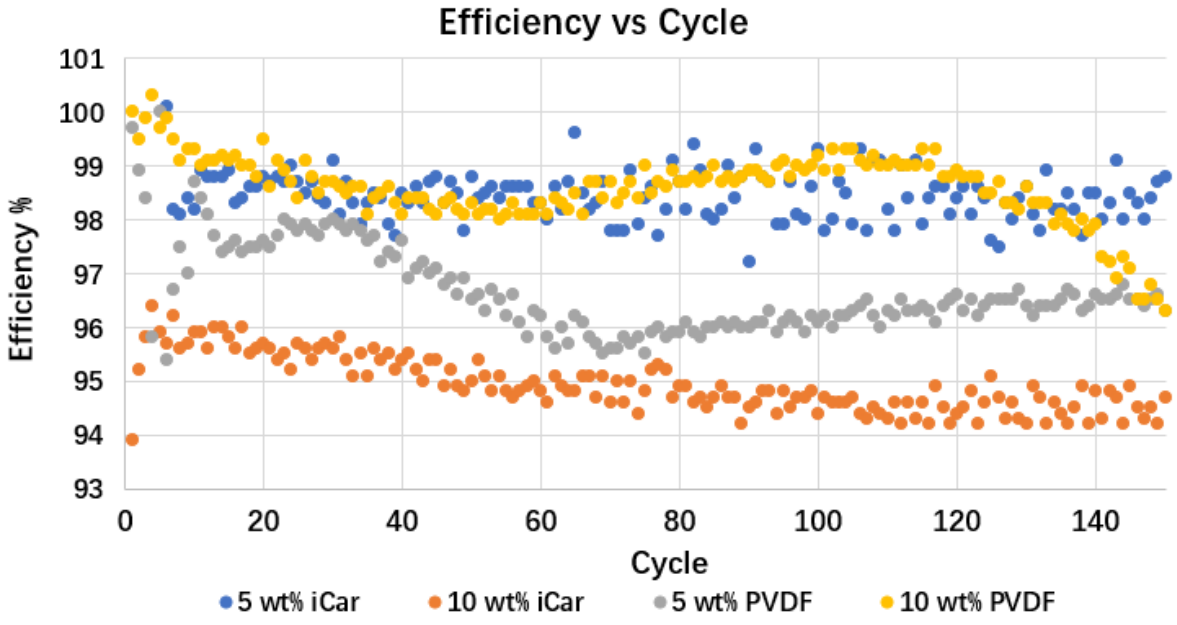

Figure 45 Cycling Efficiency of Different Cells

5 Discussion

This section would deliver discussions based on the experimental results given in Section 4 and link back to literature reviews mentioned in Section 2 and other extra references. The discussions would be categorized into different subsections based on the fabrication and testing procedures.

5.1 Carrageenan Solutions

The results founded during preparation of carrageenan solutions would be discussed in this subsection with some explanations from literature.

In Figure 15, the viscosity of 0.2% and 2.7% iCar solutions were compared before the temperature dropped to the gelling point. The viscosity would dramatically increase along with the concentration of carrageenan powder and decline with temperature [2]. The high temperature would avoid the formation of gel structure, which would cause rapid and significant increment on viscosity. As shown in Figure 13, Figure 14, Figure 16 and Figure 17, iota and kappa carrageenan both show gelation after settling down when the concentration increased from 0.2% to 2.7%. This phenomenon coincides with the description of the gelation mechanism stated by Harpell and Blakemore [49]. The gel strength is straightly proportional to the concentration and when the temperature descends below the melting point of gel between 30 °C and 70 °C, the originally random coils-shape carrageenan would intertwine together and form into three-dimensional polymer network with double helices structure as shown in Figure 6 [49].

Meanwhile, Figure 21 shows the iota carrageenan solution without thermal activation (under dissolving temperature). Many aggregated iCar lumps were observed on the wall of beaker after mixing. Both carrageenan types are soluble in water over 60 °C or with the presence of different salts and solubility could reach 7-8% [50]. It is hard for carrageenan to entirely disperse in cold water since the film layer would be generated around each carrageenan particles, forming lumped structure, and cold water cannot penetrate that layer effectively [50]. Hence, even after one-hour mixing with magnetic spinner, some carrageenan powder, covered with a transparent layer, still did not dissolve in water.

The gel formed by kappa carrageenan is stronger and more brittle than gel of iota carrageenan [50]. However, the gel structure generated by 2.7% kCar solution exhibited weaker strength than iCar solution under the same concentration (refer to Figure 14 and Figure 17). This might be caused by inherent syneresis effect of kappa carrageenan's gel [49], which will separate water out when it is contracted. Meanwhile, when the potassium ions were presented in the

kappa carrageenan, the kCar solution would gelatinize into even stronger and more brittle structure along with the concentration of potassium ion in solution as shown in Figure 18 (a) solution #6 (kCar_1wt%_80°C) (b) solution #7 (new kCar_1wt%_80°C) (c) solution #8 (new kCar_0.5wt%_80°C). The existence of large flakes of potassium ions was verified through EDS test in section 4.3.2. This phenomenon coincided with CP Kelco's statement, that potassium ions would connect double helices by the electrostatic bond between ester sulfate groups and form into gel even under 0.5% concentration [50].

By observing the inclined surfaces of carrageenan solutions across one week, both iCar and kCar solutions did not show retrogradation behavior like guar gum (GG)did. Although carrageenan and GG are both polysaccharide-based biopolymer, their gelation mechanisms are still different. Water molecules will expand and swell the particle structure of carrageenan and GG and form hydrogen bonding with hydroxyl groups in those biopolymers [47, 49]. Unlike GG molecules, which are spread in its gel state and will retrograde back to its particle state gradually due to intermolecular H-bonding during rest [47], carrageenan molecules possess stronger water-binding properties and already form into double helices structure through the existence of other ions [49]. Therefore, carrageenan solutions demonstrate constant gel structure and viscosity over one week; actually, they still will retrograde but over a long period of time.

5.2 Cathodes

Results of cathodes consisted of different carrageenan solutions were presented in Section 4.1.2 and this subsection would deliberate those outcomes by linking back to findings in the literature and conducted SEM and EDS tests. The thermogravimetric analysis (TGA) of both water and sulfur particles would be discussed as well.

5.2.1 Effect of Carrageenan Solution

The effect of carrageenan solutions' temperature had been investigated initially as presented in section 4.1.2.1. As mentioned before, the gelation effect would occur in the carrageenan solution when its temperature drops below gel point, which is around 30-70 °C [49]. Therefore, the production of two cathodes used 0.2% iCar solution in the state of 80 °C and room temperature. However, since the iCar solution with 0.2% concentration was not viscous enough to form gel texture, solution in different temperature conditions illustrated the same texture as shown in Figure 13 (1) and (2). As a result, two cathodes prepared both exhibited good attachment to the current collector, which indicated a negligible effect of solution temperature. This might be caused by gradual gelatinization of iota carrageenan as water evaporating out of

cathode during the drying process in a vacuum oven. Good dispersion of iCar particles in solution and cathode slurry made homogeneous adhesive strength within the cathode. If the concentration of solution increased until the emergence of gel structure as shown in Figure 14 (3), the temperature elevated above gelling the composition of carrageenan binder remains unchanged in the cathode, the water solvent of high concentrated solution would not be enough to dissolve active material into a slurry (see Appendix C). Therefore, a low concentrated carrageenan solution without gel structure is preferred for the cathode, which matched to the conclusion made by Cheng's team [47].

Moreover, the cathode with thermally activated carrageenan showed stronger adhesion strength than non-thermally activated one, which left granules of active material behind after punching into a disk shape (see Figure 20 (b)). This phenomenon might be caused by insufficient binder content and uneven distribution of binder in cathode slurry due to the formation of lumped particles. Hence, thermally activated carrageenan solution would generate cathode with more robust structural integrity.

As old kCar solution displayed lower viscous characteristic, the cathodes composed of 0.2% kCar solution had proven to be unqualified due to delamination of cathode layer from the current collector as demonstrated in Figure 22 (b). The weak bonding strength of this binder solution was induced by its low viscosity. A suitable adhesive agent in cathode should possess high viscosity in its aqueous solution [74]. In contrast, the new-purchased kCar powder, which formed into brittle gels due to a higher content of potassium ions, generated a cathode with aggregated active material and cracks penetrating entire layer as shown in Figure 23. The potassium ions were found in the form of compound KCl or bonded with kappa carrageenan molecules in Figure 28. This type of abnormality did not be reported by other researches yet; but the reason behind might be that the rigid hydrocolloid structure, in the form of a gel, of the kCar solution made homogeneous distribution of binder harder during the slurry mixing process. Subsequently, the strong binding connection between carrageenan molecules because of extra ions aggregated kCar coils together again during drying period, which created a shortage of binder for a portion of active material bulk. Both mechanisms had the possibility to create large cracks and isolated CNT60 material individually or simultaneously.

5.2.2 Water Evaporation and Sulfur Sublimation

An appropriate drying temperature of vacuum oven for cathodes had to be determined to evaporate all water content in cathode while retaining sulfur elements as many as possible. With absolute pressure of 20 kPa in a vacuum oven, 60 °C was not high enough to entirely eliminate moisture in the cathode, which was proven by the inadequate electrochemical performance of

the battery in Section 4.6. Discussions about vapor pressure of water and thermogravimetric analysis of sulfur element were implemented in this section to understand the effect of drying temperature on water evaporation and sulfur sublimation.

Vapor pressure measures the pressure generated by the evaporation of liquid in a sealed environment, which indicates the boiling pressure of a liquid at a specific temperature. The vapor pressure of water at 60 °C had been experimentally determined by Wexler as 19.9 kPa [75], which is lower than the vacuum oven condition in this experiment. Therefore, the evaporation rate of moisture in cathode was insufficient due to low drying temperature or high vacuum pressure as well as a complex structure of the cathode surface. While increasing the drying temperature to 70 °C, the vapor pressure of water also increases to 31.2 kPa [75], which is higher than the vacuum condition in an oven. This means that 70 °C is adequate to boil water content in the cathode, which would accelerate the evaporation speed, and remove moisture trace.

Thermogravimetric analysis (TGA) is generally used for determining physical and chemical characteristics of samples as a function of temperature by measuring the weight of the sample continuously while increasing the temperature condition [76]. Sun's team conducted a TGA for sulfur contained cathode in the atmosphere and the sublimation of sulfur element commenced around 155 °C as indicated by loss of weight. Since the drying process of the cathode was underwent vacuum state, sublimation of sulfur content would be activated at a lower temperature. Experiments done by Nash and Moses reported that the sublimation rate of sulfur element reached 10^{15} S cm^{-2} sec^{-1} at 50 °C in vacuum maintained only at 13 Pa [77]. Since the vacuum state of the drying process maintained at 20 kPa, which is extremely large compared to the condition in Nash and Moses's experiment, the sublimation effect of sulfur content in cathode was negligible. Setting temperature of the oven at 70 °C could produce valid cathodes but not guarantee for every time due to the fluctuation of oven temperature and pressure.

5.2.3 Topography and Composition

In addition to adhesion strength of binder and composition of the electronic conductor, structural characterization of cathode would also influence the electrochemical performance of the battery. Sun's group conducted LSBs with the cathode of homogeneously distributed sulfur on reduced graphene oxide and showed that well dispersed and small-size sulfur in cathode would improve the cyclability and rate capability [24]. Meanwhile, cracks in the surface of cathode would degrade the cycling performance causing by higher decaying rate [78]. Discussion is conveyed about the SEM and EDS analysis of different cathodes.

The SEM figures of iCar and PVDF based cathode were taken at low and high magnification times. Under low magnification, cathode with iCar binder presented fewer cracks and more binder content in cathode composition would also result in fewer defects. This discovery coincided with the experiment of adhesion comparison between PVDF and carrageenan binders conducted by Ling's team [4]. With more binder content, cathode surface would retain better structural characterization due to higher binding strength. Meanwhile, iCar based cathode also showed layer with better-dispersed sulfur element; yet large sulfur bulks existed in cathodes with PVDF binder. This might be caused by the hydrocolloid formation generated by iCar binder, which covered the sulfur particles in the surface layer. Hence, Figure 29 (c) and (d) presented a brighter color. The mottled effect of gelation was more evident in higher magnification images, where the cathode contents were surrounded by hydrocolloid structure. This phenomenon was consistent with results found by Cuesta's group [52].

The EDS analyses for those cathodes were presented in Section 4.5. Different types of elements could be observed via EDS technique and all cathodes showed expected elemental contents. From the elemental mappings of all cathodes, distributions of sulfur and carbon were partially overlapped, but sulfur occupied more regions in cathode surface. This can be attributed to the preparation technique of active material. By simply heating process, sulfur particles would be melted into the porous structure of CNT, but excessive sulfur would stay outside due to the limited porous volume of carbon nanotube [24]. Aluminum element was also sensed in EDS for all cathodes. This contamination might be sourced from current collector and be detected through void space in the cathode layer.

5.3 Sulfur Loading vs Thickness

While cathodes were produced, the thickness and sulfur loading of some samples were measured and calculated. Among those specimens, the highest sulfur loading reached 5.043 mg/cm^2 with 0.205 mm thickness. These data were plotted in Figure 24 and the linear relationship between thickness and sulfur loading was observed clearly. This trendline matched to the description made by Sun's team that the sulfur loading of cathode linearly increases with thickness [8]. The sulfur loading was mass of sulfur element over the area; thus, when the thickness of the cathode layer increased, it would retain more sulfur content as the area was unchanged, resulting in higher sulfur loading.

However, Figure 24 also showed some cathode samples with large deviation from the linear relationship, such as the sample with the highest sulfur loading. This might be caused by the inaccuracy of measuring apparatuses. Cathode samples were so light and thin that even little external disturbance would cause an error in measurement. At the same time, the uneven

structure of the cathode layer would also contribute to this fluctuation. As shown in Figure 30 (c), the arrangement of material in the cathode layer was not solid but left some void space or even cracks in between. Therefore, the sulfur loading was really dependent on the structural integrity of cathode.

5.4 Influence of Moisture in Cathode

The preliminary iCar based batteries showed invalid electrochemical performance in voltage profile and specific discharging capacity in Section 4.6. This was due to the trace of moisture in the cathode and this section would discuss the influence of water on the battery's performance as well as possible explanations.

The first impact generated was that it showed a sudden drop to cutoff voltage in voltage profile instead of displaying voltage plateau around 2 V as presented in Figure 7. The voltage plateau was corresponding to the electrochemical reaction between intermediate lithium polysulfides and lithium ions. It was evident that this reaction supposed to occur in LSB was substituted by another reaction. Since lithium is highly reactive with water, it might react with moisture existed in cathode rather than a sulfur element. This streaking down of voltage was in line with the experiment completed by Cui et al and excessive moisture was oxidized with the extension of voltage plateau about 1 V [79].

Another influence was that moisture would induce extremely low specific discharging capacity. This detrimental impact was the subsequent effect of low voltage plateau, where voltage plateau of reaction between water and lithium could not contribute any capacity under designated 1.6 cutoff voltage in cycling test. On the other hand, moisture would also facilitate losing of active material, increase internal resistance and promote the formation of solid electrolyte interphase in anode side [80, 81, 82]. Those adverse effects would contribute to the limited discharging capacity of LSB.

5.5 Final Batteries Comparison

The testing results of four batteries with different compositions were discussed in this section with focuses on OCV, EIS and cycling outcomes. By referring back to literature, those results would be explained with possible improvements for further investigations.

5.5.1 OCV Testing

OCV of batteries with different compositions underwent decline after cycling test as shown in Figure 41, indicating decreasing electromotive force within all batteries. This phenomenon is described as the polarisation effect, which is a change of potential between electrodes. Polarisation can be classified into two types, i.e. charge transport within electrodes and

activation of electrochemical reaction [83]. Therefore, output voltage dropping in different batteries might be accounted for various reasons, including the formation of diffusion layer between electrolyte and electrode, geometric properties of electrode and inadequate contact etc. [83]. The substantial decrease of OCV in 10 wt% PVDF battery might be caused by its poor adhesion between the cathode layer and current collector or more cycles it operated.

5.5.2 EIS Testing

As shown in Section 4.7.2, different batteries presented distinctive performances on EIS testing. Cells with 5 wt% binder had been observed with higher R_S at first when compared to cells composed of 10 wt% same types of the binder. R_S is total ohmic resistance within battery, consisting of impedance from the electrolyte, other battery components and contact between the cathode layer and current collector [84]. Since components and fabrication methods were identical for all batteries, the higher R_S might be caused by extra a 5 wt% CNT60, which induced higher electrical resistance in the cathode. Meanwhile, the batteries with iCar binder displayed lower R_S after cycling test. R_S is dependent on the electrolyte's viscosity, which would rise along with more polysulfide being dissolved [71]. Therefore, lower R_S indicated less content of dissolution of polysulfides in the electrolyte of batteries with iCar binder, which means that carrageenan binder captured the high-order polysulfide generated during the lithiation process via its sulfate leaving groups. This result also coincides the experiment conducted by Ling's group [4].

Under the same composition, batteries contained iCar binder showed higher R_{CT} after cycling test in Figure 42. R_{CT} measured the charge transfer resistance of sulfur intermediates in the cathode side, which reflects the accessibility of active material in the cathode layer by electronic conduction [71]. This may be affected by conductivity of material, morphology of the cathode layer, and porosity at cathode surface. Hence, the higher R_{CT} in iCar based batteries indicated more intermediate polysulfide existed in the cathode, which means higher discharging capacity retained. It also may be caused by anchor point provided for polysulfide to be fixed on carrageenan binder, inducing closer pathway to conductive network and uniform distribution of sulfur particles [4].

5.5.3 Cycling Test

Section 4.7.3 described electrochemical performance of all batteries in term of voltage profile and specific discharging capacity and efficiency against cycling times. All cells displayed a decreasing trend of discharging capacity along with cycle numbers; nevertheless, the first cycle of iCar based batteries showed lower capacity compared to later cycles. This may be due to the formation of hydrocolloid on the cathode surface as shown in Figure 30. This coating generated

by carrageenan binder would slow down the penetration of electrolyte into cathode during initial resting period. This phenomenon also existed in the carrageenan-based battery fabricated by Ling's group, which took 40 cycles to reach the maximum capacity with electrode of 0.2 mm thickness [4]. The cathodes used in this experiment were thinner, so electrolyte took fewer cycles to fully penetrate. Meanwhile, for the tenth and twentieth cycle, the voltage of 5 wt% PVDF battery suddenly dropped down to 1.8 V and raised back to 2 V later. It seems that electrochemical reaction from Li_2S_6 to Li_2S_2 depicted in Section 2.2 was blocked temporarily by increasing viscosity of electrolyte under relatively high current density. This phenomenon was also discovered by Yan's team, but they only showed a small reverse peak under 0.2 C rate [85].

In Figure 44, 5 wt% PVDF battery showed the highest initial specific discharging capacity with the lowest sulfur loading. Since sulfur loading was correlated to thickness as confirmed in Section 4.2, cathode with low sulfur loading tended to have a thinner layer, which was relatively readily for the electrolyte to penetrate. Therefore, more sulfur content could be utilized, resulting in a higher specific capacity. Cells composed of 5 wt% and 10 wt% PVDF binder displayed faster decaying rates, which were 47% and 43.5% after 150 cycles. On the other hand, iCar based batteries exhibited better capability of capacity retentions, which were 63% and 77% for 5 wt% and 10 wt% iCar. Higher retention rate signified alleviated polysulfide shuttling effect and less loss of active material in cathode due to replacement of traditional binder, PVDF, by carrageenan. This result was in line with the discussion of R_{CT} above. Meanwhile, more content of iCar binder also resulted in better electrochemical cyclability, with more polysulfide grafted on the binder. To capture all polysulfide, Ling's team calculated the ratio of sulfur to carrageenan to be 5/4, but they finally choose a ratio of 5/1 to balance between shuttling effect and capacity performance [4]. The highest specific discharging capacity achieved by iCar based cells were 520 mAh/g, which merely reached half capacity of battery produced by Ling's team and implied low utilization of sulfur. This might be due to the higher current density adopted in this cycling test and excessive sulfur particles isolated from conductive agent as shown in Section 4.5.2. To addressing the latter reason, longer mixing time was required to produce CNT 60 or electronic conductor could be altered with more porous structure.

In the end, iCar binder did mitigate the polysulfide shuttling effect in LSB as proven in EIS and cycling test. At the same time, its excellent adhesive strength was also confirmed in this experiment.

6 Conclusion

In this thesis project, the binder of lithium sulfur battery (LSB) was developed by replacing conventional binder PVDF with iota carrageenan (iCar). On the pathway of investigating iCar's effect on electrochemical performance, other experimental founds were also determined.

These included investigation of viscosity property of carrageenan binder solution with consideration of time impact, concentration and extra ions. It was shown that a higher concentrated solution presents higher viscosity for both iCar and kCar. The kCar binder solution, however, displayed more fluid characteristics compared to iCar binder solution under the same concentration. New kCar powder, which contained potassium ions, showed a rigid gel structure even with 0.5 wt% concentration. Meanwhile, both iCar and kCar solutions did not show retrogradation phenomenon, indicating time-independent gelation property.

The inspection of different factors potentially affecting the adhesive strength of the binder solution was also conducted. The temperature of binder solution during mixing slurry had a negligible effect on adhesion between the cathode and the current collector. The treatment temperature during fabrication, however, influenced the adhesive strength of binder solution as it required more than 60 °C to be thermally activated. On the other hand, cathode consisted of 1.75 wt% kCar binder presented poor adhesion compared to cathode with iCar binder. This discrepancy may be due to lower viscosity, caused by brittle gelation structure, of kCar solution. At the meantime, thicker cathode tended to possess higher sulfur loading.

Through SEM imaging, it was found that cathodes composed of PVDF binder showed more cracks and defects than that made of carrageenan with the same thickness. iCar based cathodes also possessed a more homogeneous dispersion of sulfur particles. These situations may be caused by stronger adhesion strength of iCar binder and its gelatinization characteristics. The EDS analyses of all cathodes displayed the presence of excessive sulfur elements without connection to conductive network.

The influence of moisture trace in cathode on battery's performance was also investigated in this project. Due to the reaction between water and lithium ions, voltage output rapidly declined under cutoff voltage limit, resulting in poor discharging capacity. Existence of moisture would also lose active material irreversibly, rise internal resistance and facilitate the formation of solid electrolyte interphase [80, 81, 82]. Those effects would further reduce the electrochemical performance of LSB.

Well-conditioned batteries with different composition of iCar binder were tested in comparison with PVDF based cells. Battery with lowest sulfur loading showed the highest specific

discharging capacity, which was 623.4 mAh/g with sulfur loading of 2.093 mg/cm^2. This battery, however, exhibited rapid decaying rate to 53% capacity retention after 150 cycles, due to adoption of PVDF binder. Although cells composed of iCar binder did not deliver most energy density, they presented better cyclability with higher capacity retention, which was increased with iCar binder content. This phenomenon indicated that polysulfide shuttling effect in LSB was alleviated through nucleophilic substitution reaction with sulfate leaving groups in iCar binder. More existence of polysulfide in iCar based cathode was also confirmed by higher R_{CT} in EIS testing.

Many unexpected issues were also discovered during this project and further research should be conducted to solve those problems. It is recommended that further research should inspect the ionic composition in kappa carrageenan powders and construct batteries with valid kCar based cathode. Investigation of drying temperature and pressure in vacuum oven was also recommended to ensure effective removal of all moisture left by aqueous solution while avoiding the sublimation of sulfur particles.

References

[1] D. Murphy, F. Di Salvo, J. Carides and J. Waszczak, "Topochemical reactions of rutile related structures with lithium," *Materials Research Bulletin,* vol. 13, no. 12, pp. 1395-1402, 1978.

[2] J. Necas and L. Bartosikova, "Carrageenan: a review," *Veterinarni Medicina,* vol. 58, no. 4, pp. 187-205, 2013.

[3] L. Miao, W. Wang, K. Yuan, Y. Yang and A. Wang, "A lithium–sulfur cathode with high sulfur loading and high capacity per area: a binder-free carbon fiber cloth–sulfur material," *Chem Commun,* vol. 50, no. 87, pp. 13231-13234, 2014.

[4] M. Ling, L. Zhang, T. Zheng, J. Feng, J. Guo, L. Mai and G. Liu, "Nucleophilic substitution between polysulfides and binders unexpectedly stabilizing lithium sulfur battery," *Nano Energy,* vol. 38, pp. 82-90, 2017.

[5] A. Manthiram, Y. Fu and Y.-S. Su, "Challenges and Prospects of Lithium–Sulfur Batteries," *Accounts of Chemical Research,* vol. 46, no. 5, pp. 1125-1134, 2012.

[6] Y. Lee, N. Choi, J. H. Park and J. K. Park, "Electrochemical performance of lithium/sulfur batteries with protected Li anodes," *Journal of Power Sources,* Vols. 119-121, pp. 964-972, 2003.

[7] S. Zhang, "Liquid electrolyte lithium/sulfur battery: Fundamental chemistry, problems, and solutions," *Journal of Power Sources,* vol. 231, pp. 153-162, 2013.

[8] K. Sun, C. A. Cama, J. Huang, Q. Zhang, S. Hwang, D. Su, A. C. Marschilok, K. J. Takeuchi, E. S. Takeuchi, H. Gan and K. Sun, "Effect of Carbon and Binder on High Sulfur Loading Electrode for Li-S Battery Technology," *Electrochimica Acta,* vol. 235, pp. 399-408, 2017.

[9] J. R. Szczech and S. Jin, "Nanostructured silicon for high capacity lithium battery anodes," *Energy & Environmental Science,* vol. 4, no. 1, pp. 56-72, 2011.

[10] D. Aurbach, Z. Lu, A. Schechter, Y. Gofer, H. Gizbar, R. Turgeman, Y. Cohen, M. Moshkovich and E. Levi, "Prototype systems for rechargeable magnesium batteries," *Nature,* vol. 407, no. 6805, pp. 724-727, 2000.

[11] M. Matsui, "Study on dlectrochemically deposited Mg metal," *Journal of Power Sources,* vol. 196, no. 16, pp. 7048-7055, 2011.

[12] H. Kim, G. Jeong, Y.-U. Kim, J.-H. Kim, C.-M. Park and H.-J. Sohn, "Metallic dnodes for next generation secondary batteries," *Chemical Society Reviews,* vol. 42, no. 23, pp. 9011-9034, 2013.

[13] J. Gao, M. Lowe, Y. Kiya and H. Abruna, "Effects of Liquid Electrolytes on the Charge–Discharge Performance of Rechargeable Lithium/Sulfur Batteries: Electrochemical and in-Situ X-ray Absorption Spectroscopic Studies," *The Journal of Physical Chemistry C,* vol. 115,

no. 50, pp. 25132-25137, 2011.

[14] D. Aurbach, E. Zinigrad, H. Teller, Y. Cohen, G. Salitra, H. Yamin, P. Dan and E. Elster, "Attempts to improve the behavior of Li electrodes in rechargeable lithium batteries," *Journal of The Electrochemical Society,* vol. 149, no. 10, pp. 1267-1277, 2002.

[15] X.-B. Cheng, C. Yan, X. Chen, C. Guan, J.-Q. Huang, H.-J. Peng, R. Zhang, S.-T. Yang and Q. Zhang, "Implantable solid electrolyte interphase in lithium-metal batteries," *Chem,* vol. 2, no. 2, pp. 258-270, 2017.

[16] K. Sun, A. K. Matarasso, R. M. Epler, X. Tong, D. Su, A. C. Marschilok, K. J. Takeuchil, E. S. Takeuchi and H. Gan, "Effect of electrolyte on high sulfur loading Li-S batteries," *Journal of The Electrochemical Society,* vol. 165, no. 2, pp. 416-423, 2018.

[17] N. Ding, X. Li, S. W. Chien, Z. Liu and Y. Zong, "In situ monitoring the viscosity change of an electrolyte in a Li–S battery," *Chemical Communications,* vol. 53, no. 73, pp. 10152-10155, 2017.

[18] Y. M. Lee, J.-W. Kim, N.-S. Choi, J. A. Lee, W.-H. Seol and J.-K. Park, "Novel Porous Separator Based on PVdF and PE Non-woven Matrix for Rechargeable Lithium Batteries," *Journal of Power Sources,* vol. 139, no. 1-2, pp. 235-241, 2005.

[19] T.-H. Cho, M. Tanaka, H. Onishi, Y. Kondo, T. Nakamura, H. Yamazaki, S. Tanase and T. Sakai, "Battery performances and thermal stability of polyacrylonitrile nano-fiber-based nonwoven separators for Li-ion battery," *Journal of Power Sources,* vol. 181, no. 1, pp. 155-160, 2008.

[20] A. Sheidaei, X. Xiao, X. Huang and J. Hitt, "Mechanical behavior of a battery separator in electrolyte solutions," *Journal of Power Sources,* vol. 196, no. 20, pp. 8728-8734, 2011.

[21] X. Huang, "Separator technologies for lithium-ion batteries," *Journal of Solid State Electrochemistry,* vol. 15, no. 4, pp. 649-662, 2010.

[22] X. Zhang, L. Ji, O. Toprakci, Y. Liang and M. Alcoutlabi, "Electrospun nanofiber-based anodes, cathodes, and separators for advanced Lithium-Ion batteries," *Polymer Reviews,* vol. 51, no. 3, pp. 239-264, 2011.

[23] S. S. Zhang, "A review on the separators of liquid electrolyte Li-ion batteries," *Journal of Power Sources,* vol. 164, no. 1, pp. 351-364, 2007.

[24] H. Sun, G.-L. Xu, Y.-F. Xu, S.-G. Sun, X. Zhang, Y. Qiu and S. Yang, "A Composite Material of Uniformly Dispersed Sulfur on Reduced Graphene Oxide: Aqueous One-Pot Synthesis, Characterization and Excellent Performance as the Cathode in Rechargeable Lithium–Sulfur Batteries," *Nano Research,* vol. 5, no. 10, p. 726–738, 2012.

[25] J. D. Navratil, Lange's handbook of chemistry, New York: McGraw-Hill, 1992.

[26] F. Jin, S. Xiao, L. Lu and Y. Wang, "Efficient Activation of High-Loading Sulfur by Small CNTs Confined Inside a Large CNT for High-Capacity and High-Rate Lithium–Sulfur Batteries,"

Nano Letters, vol. 16, no. 1, pp. 440-447, 2015.

[27] K. Saeed and I. Khan, "Carbon Nanotubes–Properties and Applications: a Review," *Carbon letters,* vol. 14, no. 3, pp. 131-144, 2013.

[28] T. W. Ebbesen, H. Lezect, H. Hiura, J. W. Bennett, H. F. Ghaem and T. Thio, "Electrical Conductivity of Individual Carbon Nanotubes," *Nature,* vol. 382, no. 6586, pp. 54-56, 1996.

[29] E. Saether, S. Frankland and R. Pipes, "Transverse Mechanical Properties of Single-walled Carbon Nanotube Crystals. Part I: Determination of Elastic Moduli," *Composites Science and Technology,* vol. 63, no. 11, pp. 1543-1550, 2003.

[30] X. Ji, K. T. Lee and L. F. Nazar, "A Highly Ordered Nanostructured Carbon–Sulphur Cathode for Lithium–Sulphur Batteries," *Nature Materials,* vol. 8, no. 6, pp. 500-506, 2009.

[31] S. Jun, S. H. Joo, R. Ryoo, M. Kruk, M. Jaroniec, Z. Liu, T. Ohsuna and O. Terasaki, "Synthesis of New, Nanoporous Carbon with Hexagonally Ordered Mesostructure," *Journal of the American Chemical Society,* vol. 122, no. 43, pp. 10712-10713, 2000.

[32] A. M. Grillet, T. Humplik, E. K. Stirrup, S. A. Roberts, D. A. Barringer, C. M. Snyder, M. R. Janvrin and C. A. Apblett, "Conductivity Degradation of Polyvinylidene Fluoride Composite Binder during Cycling: Measurements and Simulations for Lithium-Ion Batteries," *Journal of The Electrochemical Society,* vol. 163, no. 9, pp. A1859-A1871, 2016.

[33] D. Eroglu, K. R. Zavadila and K. G. Gallagher, "Critical Link between Materials Chemistry and Cell-Level Design for High Energy Density and Low Cost Lithium-Sulfur Transportation Battery," *Journal of the Electrochemical Society,* vol. 162, no. 6, pp. 982-990, 2015.

[34] J. Liu, Q. Zhang and Y.-K. Sun, "Recent progress of advanced binders for Li-S batteries," *Journal of Power Sources,* vol. 396, pp. 19-32, 2018.

[35] H. Schneider, A. Garsuch, A. Panchenko, O. Gronwald, N. Janssen and P. Novak, "Influence of different electrode compositions and binder materials on the performance of lithium–sulfur batteries," *Journal of Power Sources,* vol. 205, pp. 420-425, 2012.

[36] G. Liu, H. Zheng, A. Simens, A. Minor, X. Song and V. Battaglia, "Optimization of Acetylene Black Conductive Additive and PVDF Composition for High-Power Rechargeable Lithium-Ion Cells," *Journal of The Electrochemical Society,* vol. 154, no. 12, pp. A1129-A1134, 2007.

[37] M. Lacey, K. Edstrom and D. Brandell, "Analysis of soluble intermediates in the lithium–sulfur battery by a simple in situ electrochemical probe," *Electrochemistry Communications,* vol. 46, pp. 91-93, 2014.

[38] M. Lacey, F. Jeschull, K. Edstrom and D. Brandell, "Porosity Blocking in Highly Porous Carbon Black by PVdF Binder and Its Implications for the Li–S System," *The Journal of Physical Chemistry C,* vol. 118, no. 45, pp. 25890-25898, 2014.

[39] J. G. Lee and R. A. Bartsch, "Dehydrohalogenation by complex base. Preferential loss of "poorer" halogen leaving groups," *Journal of the American Chemical Society,* vol. 101, no.

1, pp. 228-229, 1979.

[40] W. Chen, T. Qian, J. Xiong, N. Xu, X. Liu, J. Liu, J. Zhou, X. Shen, T. Yang, Y. Chen and C. Yan, "Li-S Batteries: A New Type of Multifunctional Polar Binder: Toward Practical Application of High Energy Lithium Sulfur Batteries (Adv. Mater. 12/2017)," *Advanced Materials,* vol. 29, no. 12, 2017.

[41] M. Hagen, D. Hanselmann, K. Ahlbrecht, R. Maça, D. Gerber and J. Tübke, "Lithium–Sulfur Cells: The Gap between the State-of-the-Art and the Requirements for High Energy Battery Cells," *Advanced Energy Materials,* vol. 5, no. 16, p. 1401986, 2015.

[42] M. J. Lacey, F. Jeschull, K. Edstrom and D. Brandell, "Why PEO as a binder or polymer coating increases," *Chemical Communications,* vol. 49, no. 76, p. 8531, 2013.

[43] X. Liu, T. Murata, H. Yasuda and M. Yamachi, "Effect of Polymer Layer on the Electrochemical Performance of Lithium-Sulfur Secondary Cells in Various Organic Solvents," *GS News Tech. Rep.,* vol. 62, pp. 10-15, 2003.

[44] D. Bresser, S. Passerini and B. Scrosati, "Recent progress and remaining challenges in sulfur-based lithium secondary batteries – a review," *Chemical Communication,* vol. 49, pp. 10545-10562, 2013.

[45] E.-H. Song, J. Shang and D. Ratner, "Polysaccharides," *Polymer Science: A Comprehensive Reference,* vol. 9, pp. 137-155, 2012.

[46] J. Liu, D. G. D. Galpaya, L. Yan, M. Sun, Z. Lin, C. Yan, C. Liang and S. Zhang, "Exploiting a robust biopolymer network binder for an ultrahigh-areal-capacity Li–S battery," *Energy & Environmental Science,* vol. 10, pp. 750-755, 2017.

[47] W. Cheng, C. Cho and C. Li, "Communication—Gelatinization of Guar Gum and Its Effects on the Dispersion and Electrochemistry of Lithium-Sulfur Batteries," *Journal of The Electrochemical Society,* vol. 165, no. 10, pp. A2058-A2060, 2018.

[48] M. He, L.-X. Yuan, W.-X. Zhang, X.-L. Hu and Y.-H. Huang, "Enhanced Cyclability for Sulfur Cathode Achieved by a Water-Soluble Binder," *The Journal of Physical Chemistry C,* vol. 115, no. 31, p. 15703–15709, 2011.

[49] W. R. Blakemore and A. R. Harpell, "Carrageenan," in *Food Stabilisers, Thickeners and Gelling Agents*, New York, John Wiley & Sons, 20011, pp. 73-94.

[50] CP Kelco, Carrageenan Book, San Diego: Genu, 2001.

[51] H. Chanvrier, S. Durand, C. Garnier, G. Sworn, S. Bourriot and J.-L. Doublier, "Gelation Behaviour and Rheological Properties of K/I Hybrid Carrageenans," in *Gums and Stabilisers for the Food Industry*, Wrexham, UK, 2003.

[52] N. Cuesta, A. Ramos, I. Cameán, C. Antuña and A. B. García, "Hydrocolloids as binders for graphite anodes of lithium-ion batteries," *Electrochimica Acta,* vol. 155, pp. 140-147, 2014.

[53] C. A. Ng and D. H. Camacho, "Polymer electrolyte system based on carrageenan-poly(3,4-ethylenedioxythiophene) (PEDOT) composite for dye sensitized solar cell," *IOP Conference Series: Materials Science and Engineering,* vol. 79, 2015.

[54] V. Moniha, M. Alagar, S. Selvasekarapandian, B. Sundaresan and G. Boopathi, "Conductive bio-polymer electrolyte iota-carrageenan with ammonium nitrate for application in electrochemical devices," *Journal of Non-Crystalline Solids,* vol. 481, p. 424–434, 2018.

[55] W. Zhu, X. Wang, B. Yang and X. Tang, "A novel ionic-conduction mechanism based on polyurethane electrolyte," *Journal of Polymer Science Part B: Polymer Physics,* vol. 39, no. 11, pp. 1246-1254, 2001.

[56] P. Bruce, S. Freunberger, L. Hardwick and J. Tarascon, "Li–O2 and Li–S batteries with high energy storage," *Nature Materials,* vol. 11, no. 1, pp. 19-29, 2012.

[57] A. Manthiram, Y. Fu, S. Chung, C. Zu and Y. Su, "Rechargeable Lithium–Sulfur Batteries," *Chemical Reviews,* vol. 114, no. 23, pp. 11751-11787, 2014.

[58] H. Cheng and S. Wang, "Recent progress in polymer/sulphur composites as cathodes for rechargeable lithium–sulphur batteries," *Journal of Materials Chemistry A,* vol. 2, p. 13783–13794, 2014.

[59] L. Chen and L. Shaw, "Recent advances in lithium–sulfur batteries," *Journal of Power Sources,* vol. 267, pp. 770-783, 2014.

[60] C. Liang, N. J. Dudney and J. Y. Howe, "Hierarchically Structured Sulfur/Carbon Nanocomposite Material for High-Energy Lithium Battery," *Chemistry of Material,* vol. 21, no. 19, p. 4724–4730, 2009.

[61] H. S. Ryu, J. W. Park, J. Park, J.-p. Ahn, K.-w. Kim, J.-h. Ahn, T.-h. Nam, G. Wang and H.-j. Ahn, "High capacity cathode materials for LiS batteries," *Journal of Materials Chemistry A,* vol. 1, no. 5, pp. 1573-1578, 2013.

[62] W. Zhou, Y. Yu, H. Chen, F. J. Disalvo and H. D. Abruña, "Yolk-shell structure of polyaniline-coated sulfur for lithium-sulfur batteries," *Journal of the American Chemical Society,* vol. 135, no. 44, pp. 16736-16743, 2013.

[63] V. Kolosnitsyn and E. Karaseva, "Lithium-sulfur batteries: Problems and solutions," *Russian Journal of Electrochemistry,* vol. 44, no. 5, pp. 506-509, 2008.

[64] A. Freitag, M. Stamm and L. Ionov, "Separator for lithium-sulfur battery based on polymer blend membrane," *Journal of Power Sources,* vol. 363, pp. 384-391, 2017.

[65] T. Zhao, Y. Ye, C. Lao, G. Divitini, P. R. Coxon, X. Peng, X. He, H. Kim, K. Xi, C. Ducati, R. Chen, Y. Liu, S. Ramakrishna and R. V. Kumar, "A Praline-Like Flexible Interlayer with Highly Mounted Polysulfide Anchors for Lithium–Sulfur Batteries," *Small,* vol. 13, p. 1700357, 2017.

[66] E. Peled, "The Electrochemical Behavior of Alkali and Alkaline Earth Metals in Nonaqueous Battery Systems—The Solid Electrolyte Interphase Model," *Journal of The Electrochemical*

Society, vol. 126, no. 12, p. 2047, 1979.

[67] H. Kim, G. Jeong, Y. Kim, J. Kim, C. Park and H. Sohn, "Metallic anodes for next generation secondary batteries," *Chemical Society Reviews,* vol. 42, no. 23, p. 9011, 2013.

[68] D. Aurbach, "Review of selected electrode–solution interactions which determine the performance of Li and Li ion batteries," *Journal of Power Sources,* vol. 89, no. 2, pp. 206-218, 2000.

[69] Y.-Q. Lu, J.-T. Li, X.-X. Peng, T. Zhang, Y.-P. Deng, Z.-Y. Wu, L. Deng, L. Huang, X.-D. Zhou and S.-G. Sun, "Achieving high capacity retention in lithium-sulfur batteries with an aqueous binder," *Electrochemistry Communications,* vol. 72, pp. 79-82, 2016.

[70] Y. V. Mikhaylik, I. Kovalev, R. Schock, K. Kumaresan, J. Xu and J. Affinito, "High Energy Rechargeable Li-S Cells for EV Application: Status, Remaining Problems and Solutions," *ECS Trans.,* vol. 25, no. 35, pp. 23-34, 2010.

[71] N. A. Ca˜nas, K. Hirose, B. Pascucci, N. Wagner, K. A. Friedrich and R. Hiesgen, "Investigations of lithium–sulfur batteries using electrochemical impedance spectroscopy," *Electrochimica Acta,* vol. 97, p. 42– 51, 2013.

[72] Z. Deng, Z. Zhang, Y. Lai, J. Liu, J. Li and Y. Liu, "Electrochemical Impedance Spectroscopy Study of a Lithium/Sulfur Battery: Modeling and Analysis of Capacity Fading," *Journal of The Electrochemical Society,* vol. 160, no. 4, pp. A553-A558, 2013.

[73] Y. F. Pulido, C. Blanco, D. Anseán, V. M. García, F. Ferrero and M. Valledor, "Determination of suitable parameters for battery analysis by Electrochemical Impedance Spectroscopy," *Measurement,* vol. 106, pp. 1-11, 2017.

[74] M. Bele, K. Kocˇevar, I. Musˇevic, J. Besenhard and S. Pejovnik, "Substrate-induced deposition of carbon black particles from aqueous dispersion on gelatin-modified surface," *Colloids and Surfaces A: Physicochemical and Engineering Aspects,* vol. 168, p. 231–239, 2000.

[75] A. Wexler, "Vapor Pressure Formulation for Water in Range 0 to 100 °C," *J. Res. Natl. Bur. Stand. A,* vol. 80, pp. 775-785, 1976.

[76] Q.-V. Bach and W.-H. Chen, "Pyrolysis characteristics and kinetics of microalgae via thermogravimetric analysis (TGA): A state-of-the-art review," *Bioresource Technology,* vol. 246, pp. 88-100, 2017.

[77] D. B. Nash and J. I. Moses, "VACUUM WEATHERING OF SULFUR: TEMPERATURE EFFECTS AND APPLICATIONS TO IO," *Geophysical Research Letters,* vol. 15, no. 7, pp. 697-700, 1988.

[78] D. J. Miller, C. Proff, J. G. Wen, D. P. Abraham and J. Bareño, "Observation of Microstructural Evolution in Li Battery Cathode Oxide Particles by In Situ Electron Microscopy," *Advanced Energy Materials,* vol. 3, p. 1098–1103, 2013.

[79] X. Cui, F. Tang, Y. Zhang, C. Li, D. Zhao, F. Zhou, S. Li and H. Feng, "Influences of trace water on electrochemical performances for lithium hexafluoro phosphate- and lithium Bis(oxalato)borate-based electrolytes," *Electrochimica Acta,* vol. 273, pp. 191-199, 2018.

[80] H. F. and Z. Y. H., "Review of electrolytes for lithium-ion batteries," *J. Battery Bimonthly,* vol. 31, pp. 290-293, 2001.

[81] P. M. B., "Theory of SEI formation in rechargeable batteries: capacity Fade, accelerated aging and lifetime prediction," *J. Electrochemical Society,* vol. 160, pp. 243-246, 2013.

[82] N. M. Y., "Role of lithium salt on solid electrolyte interface (SEI) formation and structure in lithium ion batteries," *J. Electrochemical Society,* vol. 161, pp. 1001-1006, 2016.

[83] B. Yana, C. Lim, Z. Song and L. Zhu, "Analysis of Polarization in Realistic Li Ion Battery Electrode Microstructure Using Numerical Simulation," *Electrochimica Acta,* vol. 185, p. 125–141, 2015.

[84] T. Reddy and D. Linden, Linden's handbook of batteries 4th ed., New York: McGraw-Hill, 2011.

[85] J. Yan, X. Liu and B. Li, "Capacity Fade Analysis of Sulfur Cathodes in Lithium–Sulfur Batteries," *Advanced Science,* vol. 3, no. 12, p. n/a, 2016.

[86] F. Orsini, D. Pasquier, B. Beaudoin, J. Tarascon, M. Trentin, N. Langenhuizen, E. D. Beer and P. Notten, "In situ Scanning Electron Microscopy SEM Observation of Interfaces within Plastic Lithium Batteries," *Journal of Power Sources,* vol. 76, no. 1, pp. 19-29, 1998.

[87] S. Spirk, Polysaccharides as Battery Components, Graz: Springer, 2018.

[88] Y. Fu and A. Manthiram, "Orthorhombic Bipyramidal Sulfur Coated with Polypyrrole Nanolayers As a Cathode Material for Lithium–Sulfur Batteries," *The Journal of Physical Chemistry C,* vol. 116, p. 8910–8915, 2012.

Appendix A: Equation of Calculating Thickness of Cathode:

$$t_{cathode} = t_{total} - t_{current\ collector}$$

Where:

$t_{cathode}$ is the thickness of cathode that we interested in $[mm]$;

t_{total} is the total thickness measured from screw gauge in $[mm]$; and

$t_{current\ collector}$ is the thickness of current collector measured from screw gauge in $[mm]$.

And the thickness of carbon coated aluminum foil and pure aluminum foil is:

- $t_{carbon\ coated} = 0.018\ mm$
- $t_{aluminum\ foil} = 0.016\ mm$

Appendix B: Raw Data of Thickness and Sulfur Loading

The raw data of thickness and sulfur loading of cathode is presented in Table 6.

Table 6 Raw data of thickness and SL

8:1:1			8.5:1:0.5		
CC Type	Thickness (mm)	SL	CC Type	Thickness (mm)	SL
CCAF	0.232	3.715	AF	0.165	3.875
CCAF	0.152	4.01	AF	0.205	5.043
CCAF	0.076	1.604	AF	0.132	3.216
CCAF	0.079	2.1486	CCAF	0.139	3.145
CCAF	0.079	2.244	CCAF	0.14	3.226
CCAF	0.081	2.311	CCAF	0.148	3.348
CCAF	0.081	2.387	CCAF	0.155	3.308
AF	0.142	3.82	CCAF	0.089	2.567
AF	0.141	3.62	CCAF	0.068	1.765
AF	0.136	3.4473	CCAF	0.079	1.938
AF	0.137	3.457	CCAF	0.097	2.5873
AF	0.136	3.5237	AF	0.117	2.441
AF	0.132	3.3136	AF	0.131	2.681
AF	0.091	2.01	AF	0.11	2.2654
AF	0.09	1.87	AF	0.133	3.038
AF	0.095	2.242	AF	0.123	2.5057
AF	0.095	1.857	AF	0.138	3.025
AF	0.1	2.2177	AF	0.165	3.5576
AF	0.091	1.8694	AF	0.158	3.4083
			AF	0.169	3.525
			AF	0.15	3.181

Appendix C: Slurry Mixing with Highly Concentrated Binder Solution